

University of Windsor

## Scholarship at UWindor

---

Electronic Theses and Dissertations

Theses, Dissertations, and Major Papers

---

2018

# Shear Transfer Mechanism in FRP Reinforced Composite Concrete Structures

MOFRHE S. ALRUWAILI  
*University of Windsor*

Follow this and additional works at: <https://scholar.uwindsor.ca/etd>

---

### Recommended Citation

ALRUWAILI, MOFRHE S., "Shear Transfer Mechanism in FRP Reinforced Composite Concrete Structures" (2018). *Electronic Theses and Dissertations*. 7345.  
<https://scholar.uwindsor.ca/etd/7345>

This online database contains the full-text of PhD dissertations and Masters' theses of University of Windsor students from 1954 forward. These documents are made available for personal study and research purposes only, in accordance with the Canadian Copyright Act and the Creative Commons license—CC BY-NC-ND (Attribution, Non-Commercial, No Derivative Works). Under this license, works must always be attributed to the copyright holder (original author), cannot be used for any commercial purposes, and may not be altered. Any other use would require the permission of the copyright holder. Students may inquire about withdrawing their dissertation and/or thesis from this database. For additional inquiries, please contact the repository administrator via email ([scholarship@uwindsor.ca](mailto:scholarship@uwindsor.ca)) or by telephone at 519-253-3000ext. 3208.

# **Shear Transfer Mechanism in FRP Reinforced Composite Concrete Structures**

By

**Mofrhe S. Alruwaili**

A Thesis  
Submitted to the Faculty of Graduate Studies  
through the Department of Civil & Environmental Engineering  
in Partial Fulfillment of the Requirements for  
the Degree of Master of Applied Science at the  
University of Windsor

Windsor, Ontario, Canada

2018

© 2018 Mofrhe S. Alruwaili

# **Shear Transfer Mechanism in FRP Reinforced Composite Concrete Structures**

By

**Mofrhe S. Alruwaili**

APPROVED BY:

---

M. Abdelkhalek  
Department of Electrical and Computer Engineering

---

S. Cheng  
Department of Civil and Environmental Engineering

---

F. Ghrib, Advisor  
Department of Civil and Environmental Engineering

---

A. El-Ragaby, Co-Advisor  
Department of Civil and Environmental Engineering

December 18, 2017

## **DECLARATION OF ORIGINALITY**

I hereby certify that I am the sole author of this thesis and that no part of this thesis has been published or submitted for publication.

I certify that, to the best of my knowledge, my thesis does not infringe upon anyone's copyright nor violate any proprietary rights and that any ideas, techniques, quotations, or any other material from the work of other people included in my thesis, published or otherwise, are fully acknowledged in accordance with the standard referencing practices. Furthermore, to the extent that I have included copyrighted material that surpasses the bounds of fair dealing within the meaning of the Canada Copyright Act, I certify that I have obtained a written permission from the copyright owner(s) to include such material(s) in my thesis and have included copies of such copyright clearances to my appendix.

I declare that this is a true copy of my thesis, including any final revisions, as approved by my thesis committee and the Graduate Studies office, and that this thesis has not been submitted for a higher degree to any other University or Institution.

## ABSTRACT

Composite construction in which precast girders and cast-in-place slabs are combined together is a widely used methodology especially in bridge construction. To maintain continuity at the slab-girder joints, steel reinforcement across these joints has always been used. Under the influence of extreme weather and traffic conditions, the steel reinforcement crossing these joints would be subjected to extensive corrosion. This would deteriorate the connection strength and subsequently the girder-slab composite action is reduced. Glass Fiber-Reinforced Polymer (GFRP) is an elastic, non-corrodible, strong and lightweight material that has been shown to be a good alternative to steel in many reinforced concrete applications. This study is the second phase of an ongoing research project at the University of Windsor to evaluate the performance of GFRP as a shear transfer reinforcement. The experimental program involved constructing and testing twenty push-off test specimens. Each specimen consisted of two connected L-shaped concrete blocks, cast at different times. The interface surface between the blocks was left as-cast and intersected by the GFRP reinforcement. In addition, control specimens containing steel and others with no reinforcement across their interfaces were used. The test parameters of the research included the reinforcement stiffness and the shape of the GFRP reinforcement. The data collected were the ultimate strength, the slip and the reinforcement strain. The test results of the specimens confirmed the feasibility and effectiveness of the GFRP shear transfer reinforcement at higher reinforcement contents.

**Keywords:** Shear transfer, Shear friction, GFRP, Composite construction, Connections, Push-off specimens.

## **ACKNOWLEDGEMENTS**

The author would like to thank God for blessings and giving him the patience to finish his research.

The author would like to express his deepest gratitude and appreciation to:

1. His supervisors, Dr. Amr El Ragaby and Dr. Faouzi Ghrib for their constant support and guidance throughout his study during the entire research program.
2. His committee members, Dr. M. Abdelkhalek and Dr. S. Cheng.
3. His graduate colleagues for their help during his lab preparation and test program.
4. The technical staff of the Structural Laboratory of the Department of Civil and Environmental Engineering at the University of Windsor for their help during his lab works.
5. Pultrall Inc. for their support by providing the GFRP materials, which is deeply appreciated and acknowledged.
6. His parents, brothers, and sisters for their constant support during his research program; this is greatly valued.

In addition, the author would like to express his honest and extreme thanks to his family, the two little kids (Haitham and Sulafa), and his beloved wife for her constant support, patience, and encouragement, which are extremely valued and appreciated.

The author would like to express his deep gratitude and appreciation to the Ministry of Higher education of Saudi Arabia represented by the Saudi Bureau in Ottawa for their financial support.

The author also expresses his thanks and appreciation to the Saudi Government represented by the Saudi Embassy in Ottawa for their help during his study and residence in Canada.

## TABLE OF CONTENTS

DECLARATION OF ORIGINALITY .....	iii
ABSTRACT .....	iv
ACKNOWLEDGEMENTS .....	v
LIST OF TABLES .....	x
LIST OF FIGURES .....	xi
LIST OF SYMBOLS .....	xiv
CHAPTER 1	
INTRODUCTION .....	1
1.1 General .....	1
1.2 Motivation .....	3
1.3 Objective .....	4
1.4 Scope .....	4
1.5 Thesis Organization .....	5
CHAPTER 2	
LITERATURE REVIEW .....	6
2.1 Background .....	6
2.2 Horizontal Shear in Composite beams .....	9
2.3 Review of Shear Transfer Models .....	13
2.3.1 Linear Shear Transfer Models .....	14
2.3.1.1 Birkeland and Birkeland, 1966 .....	14
2.3.1.2 Mast, 1968 .....	15
2.3.1.3 Mattock and Hawkins, 1972 .....	15

2.3.1.4 Mattock, 1974 .....	17
2.3.1.5 Hermansen and Cowan, 1974 .....	18
2.3.1.6 Mattock, Li and Wang, 1976 .....	18
2.3.1.7 Mattock, 1988 .....	19
2.3.1.8 Patnaik, 2001 .....	19
2.3.1.9 Mattock, 2001 .....	20
2.3.1.10 Khan and Mitchell, 2002 .....	21
2.3.1.11 Harries, Zeno and Shahrooz, 2012 .....	22
2.3.1.12 Alkatan, 2016 .....	23
2.3.2 Nonlinear Shear Transfer Models .....	24
2.3.2.1 Birkeland, 1968 .....	24
2.3.2.2 Raths, 1977 .....	24
2.3.2.3 Loov, 1978 .....	25
2.3.2.4 Walraven, Frénay and Pruijssers, 1987 .....	25
2.3.2.5 Mau and Hsu, 1988 .....	26
2.3.2.6 Loov and Patnaik, 1994 .....	26
2.3.2.7 Mattock, 1994 .....	27
2.3.2.8 Ali and White, 1999 .....	28
2.3.2.9 Mansur, Vinayagam and Tan, 2008 .....	28
2.4 Shear Transfer Provisions in Existing Design Codes and Standards .....	29
2.4.1 AASHTO Standard Specifications for Highway Bridges, 2002 .....	30
2.4.2 Canadian Design Code of Concrete Structures, CAN/CSA A23.3, 2014 .....	30
2.4.3 Canadian Bridge and Highway Design Code, CAN/CSA S6, 2014 .....	31



2.4.4 American Concrete Institute Code Requirements for Structural Concrete, ACI 318, 2014 .....	32
2.5 Summary .....	34
CHAPTER 3	
EXPERIMENTAL PROGRAM .....	36
3.1 Introduction .....	36
3.2 Test Specimens .....	37
3.3 Fabrication of the Push-off Specimens .....	41
3.4 Materials Properties .....	49
3.4.1 Steel Reinforcement .....	49
3.4.2 GFRP Reinforcement .....	50
3.4.3 Concrete .....	51
3.5 Instrumentations .....	51
3.5.1 Shear Slip .....	51
3.5.2 Reinforcement Strain Monitoring .....	53
3.6 Setup and Testing .....	55
3.7 Summary .....	57
CHAPTER 4	
EXPERIMENTAL RESULTS AND DISCUSSION .....	58
4.1 Introduction .....	58
4.2 Analysis of Test Results .....	59
4.2.1 Load-Slip Behavior .....	60
4.2.2 Load-Reinforcement Strain Behavior .....	66
4.2.3 Effect of Reinforcement Stiffness Parameter .....	71

4.2.4 Failure Modes .....	75
4.2.5 Ultimate Strength .....	82
4.3 Summary .....	85
CHAPTER 5	
CONCLUSIONS AND RECOMMENDATIONS .....	86
5.1 General .....	86
5.2 Conclusions .....	87
5.3 Future Work .....	88
REFERENCES .....	89
VITA AUCTORIS .....	94

## LIST OF TABLES

<b>Table 2.1</b> Shear transfer Design Expressions .....	33
<b>Table 3.1</b> Test matrix .....	41
<b>Table 3.2</b> Properties of GFRP reinforcement .....	50
<b>Table 4.1</b> Test results .....	59
<b>Table 4.2</b> Groups of specimens having similar reinforcement shape and stiffness parameter .....	71
<b>Table 4.3</b> Groups of specimens having different reinforcement shape and similar stiffness parameter .....	72
<b>Table 4.4</b> Test results arranged ascendingly according to the reinforcement stiffness Parameter .....	74

## LIST OF FIGURES

<b>Figure 1.1</b> Composite steel-concrete beam .....	2
<b>Figure 1.2</b> Typical composite concrete beam (precast girder combined with cast-in-place Slab) .....	2
<b>Figure 2.1</b> Shear friction hypothesis (Birkeland and Birkeland, 1966) .....	8
<b>Figure 2.2</b> Shear transfer in initially uncracked concrete (Mattock and Hawkins, 1972) .....	8
<b>Figure 2.3</b> Development of horizontal shear stresses .....	10
<b>Figure 2.4</b> (a) precast beam and cast-in-place slab, (b) composite-section and (c) non- composite section .....	11
<b>Figure 2.5</b> Evaluation of the interface longitudinal shear .....	13
<b>Figure 2.6</b> Push-off specimens: (a) Push-off; (b) Pull-off; (c) Modified push-off (Mattock and Hawkins, 1972) .....	15
<b>Figure 2.7</b> Push-off test specimens with orthogonal and parallel reinforcement (Mattock, 1974) .....	17
<b>Figure 3.1</b> Design configuration of push-off specimens .....	38
<b>Figure 3.2</b> Shapes of GFRP reinforcement .....	40
<b>Figure 3.3</b> Wooden Formworks .....	42
<b>Figure 3.4</b> Steel cages .....	43
<b>Figure 3.5</b> Steel cages installed for the first halves of 4 specimens before concrete casting .....	44
<b>Figure 3.6</b> Shear transfer reinforcement secured to the steel cages of first specimen's halves before concrete casting .....	44

<b>Figure 3.7</b> Cast of first blocks and the shear reinforcement is extended from the top surfaces prior to casting second specimen's blocks .....	45
<b>Figure 3.8</b> Steel cages of top blocks installed in formworks .....	46
<b>Figure 3.9</b> Cast of top concrete .....	47
<b>Figure 3.10</b> Specimens moist curing .....	48
<b>Figure 3.11</b> Final shape of the test push-off specimen .....	49
<b>Figure 3.12</b> The used linear variable differential transducer (LVDT) .....	52
<b>Figure 3.13</b> The LVDT mounted to the surface of the specimen .....	53
<b>Figure 3.14</b> Electronic strain gauge glued to the surface of GFRP bar .....	54
<b>Figure 3.15</b> Schematic drawing of the test setup .....	56
<b>Figure 3.16</b> Test set-up .....	56
<b>Figure 4.1</b> Load-Slip behavior of specimens of series A1 with stirrups shear transfer reinforcement and unreinforced specimen .....	61
<b>Figure 4.2</b> Load-Slip behavior of specimens of series A2 with stirrups shear transfer reinforcement and unreinforced specimen .....	61
<b>Figure 4.3</b> Load-Slip behavior of specimens of series A1 with headed bars shear transfer reinforcement and unreinforced specimen .....	63
<b>Figure 4.4</b> Load-Slip behavior of specimens of series A2 with headed bars shear transfer reinforcement and unreinforced specimen .....	63
<b>Figure 4.5</b> General load-slip behavior (Alkatan 2016) .....	65
<b>Figure 4.6</b> Load-Strain behavior of specimens SS2-A1 and SS2-A2 .....	66
<b>Figure 4.7</b> Load-Reinforcement Strain behavior of specimens with GFRP stirrups of series A1 .....	69

<b>Figure 4.8</b> Load-Reinforcement Strain behavior of specimens with GFRP stirrups of series A2 .....	69
<b>Figure 4.9</b> Load-Reinforcement Strain behavior of specimens with GFRP headed bars of series A1.....	70
<b>Figure 4.10</b> Load-Reinforcement Strain behavior of specimens with GFRP headed bars of series A2 .....	70
<b>Figure 4.11</b> Failure mode of unreinforced specimen C0-A2 .....	75
<b>Figure 4.12</b> Splitting of specimen C0-A1.....	76
<b>Figure 4.13</b> Concrete spalling in specimen SS2-A1.....	77
<b>Figure 4.14</b> Concrete spalling in specimen SS2-A2 .....	77
<b>Figure 4.15</b> Concrete spalling in specimen FS2-A1.....	78
<b>Figure 4.16</b> Concrete spalling in specimen FS3-A1.....	79
<b>Figure 4.17</b> Failure mode of specimen FH6-A2.....	80
<b>Figure 4.18</b> Rupture of headed bars in specimen FH6-A1.....	81
<b>Figure 4.19</b> Test results and Eq. 4.2.....	84

## LIST OF SYMBOLS

$A_{cv}$	=	area of the concrete section resisting shear transfer
$A_v$	=	area of the reinforcement crossing the shear plane
$A_s$	=	area of the longitudinal steel reinforcement
$a$	=	equation parameter (Ali and White, 1999)
$b$	=	equation parameter (Ali and White, 1999)
$b$	=	width of the cross section at the level under consideration
$c$	=	cohesion stress of the interface surface in MPa
$C_1$	=	equation parameter (Walraven, Frénay and Pruijssers, 1987)
$C_2$	=	equation parameter (Walraven, Frénay and Pruijssers, 1987)
$C_f$	=	total factored compressive force in the cast-in-place slab along the considered beam segment
$C_s$	=	the influence of the concrete density (Raths, 1977)
$d$	=	effective depth of the beam cross section
$E$	=	modulus of elasticity
$E_F$	=	modulus of elasticity of GFRP reinforcement
$E_s$	=	modulus of elasticity of steel reinforcement
$f'_c$	=	concrete compressive strength
$f'_{cc}$	=	the concrete compressive strength of 150 mm (5.9 in) cubes ( $f'_c = 0.85f'_{cc}$ )
$f_s$	=	the stress in the reinforcement
$f_y$	=	yield strength of the steel reinforcement crossing the shear plane
$f_{Fu}$	=	ultimate tensile strength of GFRP reinforcement
$I$	=	moment of inertia of the entire uncracked cross section
$k$	=	constant in Loov's parabolic equation (Loov, 1978)
$k$	=	constant in Loov and Patnaik's equation (Loov and Patnaik, 1994)
$K_1$	=	equation parameter (Mattock, 2001)
$K_2$	=	equation parameter (Mattock, 2001)
$K_3$	=	equation parameter (Mattock, 2001)
$l$	=	length of the interface of the horizontal shear transfer
$N$	=	unfactored permanent load perpendicular to the shear plane (positive if

		compression and negative if tension)
$P$	=	unfactored permanent concentrated load perpendicular to the shear plane (positive if compression and negative if tension)
$Q$	=	first moment of the area above or below the level of the cross section under consideration with respect to the natural axis of the section
$T_f$	=	total factored tensile force in the longitudinal reinforcement
$v_l$	=	longitudinal shear stress
$v_u$	=	ultimate shear transfer strength MPa
$V_u$	=	ultimate shear transfer strength KN
$V$	=	shear force at the section under consideration
$V_f$	=	factored shear force at the section under consideration
$W$	=	unfactored permanent distributed load
$\alpha$	=	equation parameter (Harries, Zeno and Shahrooz, 2012)
$\alpha_f$	=	angle between the shear plane and the shear friction reinforcement
$\varepsilon_F$	=	strain in the GFRP reinforcement at ultimate shear transfer load
$\varepsilon_{Fu}$	=	ultimate tensile strain of GFRP reinforcement
$\theta$	=	angle between the shear plane and the reinforcement crossing the shear plane (Mattock, 1974)
$\lambda$	=	factor to account for low-density concrete
$\mu$	=	coefficient of friction
$\rho_v$	=	reinforcement ratio of the reinforcement crossing the shear plane ( $A_v/A_{cv}$ )
$\rho_{v,min}$	=	minimum ratio of the reinforcement crossing the shear plane
$\rho_v f_y$	=	reinforcement parameter
$E \rho_v$	=	reinforcement parameter
$\sigma$	=	total compressive stress to the shear plane ( $\rho_v f_y + \sigma_n$ )
$\sigma_n$	=	externally applied normal stress ( $N/A_{cv}$ )
$\emptyset$	=	angle of internal friction



# **CHAPTER 1**

## **INTRODUCTION**

### **1.1 General**

Composite beams usually refer to beams fabricated with a combination of different construction materials such as that shown in Figure 1.1 consisting of a concrete slab provided on top of a steel beam. In recent reinforced concrete applications, composite concrete beams in which precast concrete girders are combined with cast-in-place concrete slabs are very well known and used in the construction industry, particularly, in highway bridge construction (Figure 1.2). Composite concrete construction is an effective construction methodology that allows to combine precast and in-situ concretes while retaining continuity and efficiency of the monolithic construction. It permits to utilize the overall strength and stiffness of the composite beam resulting in lighter and shallower beams and, hence, an overall cost savings.

Despite the obvious benefits of using composite concrete beams, if the in situ-cast slab or deck is to be considered in the design, the shear stresses imposed at the girder-slab interface level must be transferred efficiently between the two elements. In a fully composite concrete beam, all the interfacial shear stresses resulting from bending are transmitted between the girder and the slab at their joint.

To achieve continuity, steel reinforcement crossing the interface surface between the combined prefabricated girders and their cast-in-place flanges is being used. However, deterioration of the deck slab due to harsh environmental and loading conditions results in corrosion of the steel, especially when de-icing salt is used. To avoid this issue, epoxy

coated steel reinforcement was proposed to be used as an alternative to black steel in bridge construction, but it was shown to be impractical to eliminate the corrosion problem or to reduce the long-term maintenance cost (Pianca et al. 2005).

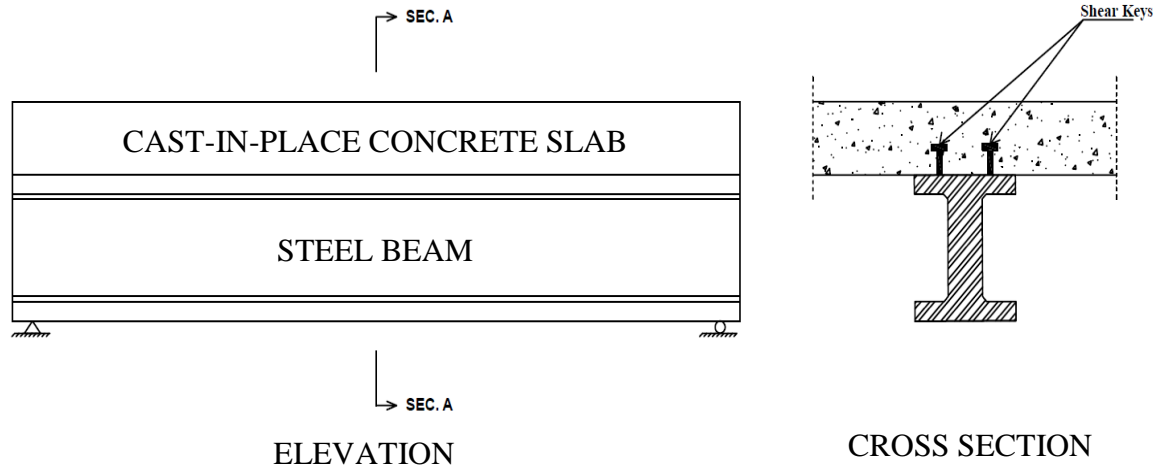


**Figure 1.1** Composite steel-concrete beam

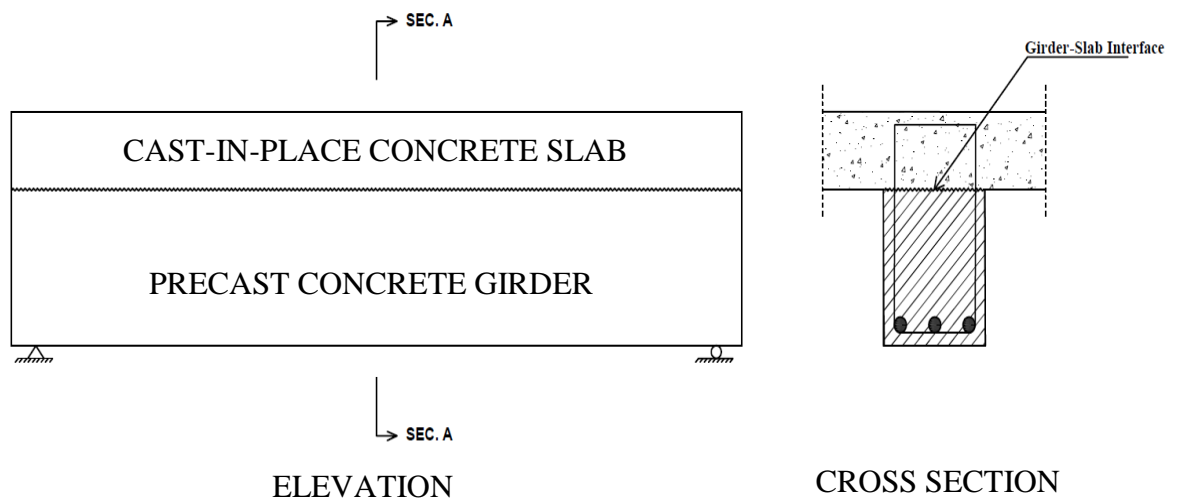


**Figure 1.2** Typical composite concrete beam (precast girder combined with cast-in-place Slab)

Fiber Reinforced Polymers (FRPs) are relatively new construction materials that have shown to be an effective substitute to steel in many reinforced concrete applications, particularly Glass-FRP. FRPs are nonconductive, noncorrodible and have high tensile and bond strengths, in addition to their light weight; about 75% less than steel. These properties encouraged their application in reinforced concrete structures. To evaluate the performance of the GFRP reinforcement across concrete joints of composite concrete beams, an ongoing research was launched at the University of Windsor, which this study represents the second part of it. In the first part of this research (Alkatan, 2016), GFRP stirrups, headed bars and bent bars were used. The GFRP reinforcement stiffness parameter ( $E\rho_v$ ) among the specimens of the first part was in the range of 0 to 304 MPa. In the current study, the application of GFRP reinforcement was further explored for higher stiffness parameters, up to 811 MPa. It was suggested by Alkatan (2016) that if GFRP reinforcement is to be used across concrete-to-concrete joints, it should have a minimum stiffness parameter ( $E\rho_v$ ) of 203 MPa in order to activate the shear transfer resistance.

## **1.2 Motivation**

Glass Fiber Reinforced Polymer (GFRP) is a fairly new construction material that is strong, light and non-corrosive. GFRP has emerged over the past twenty years in concrete structural applications. GFRP was shown to be an outstanding alternative to the traditional steel as flexural and shear reinforcement. To explore the feasibility of the new application of the Fiber Reinforced Polymers, FRP, as a shear transfer reinforcement across concrete-to-concrete connections, a research program started at the Department of Civil and Environmental Engineering at the University of Windsor. The primary results of the first

part of this study showed the effectiveness of GFRP in this application (Alkatan, 2016). However, the objective of this research is to further explore the behavior of Glass Fiber Reinforced Polymers (GFRP) reinforcement as a shear transfer reinforcement along the junctions of precast girders and cast-in-place slabs, for higher reinforcement contents, and to provide the related design guidelines and recommendations.

### **1.3 Objective**

The objective of this study is to extend the investigation of the shear transfer behavior of interfaces between concretes cast at different times (cold-joint), when GFRP is utilized as a shear transfer reinforcement. The present research which is to extend the work of (Alkatan, 2016) to study the interface response for higher values of the GFRP reinforcement stiffness and the reinforcement shape on the shear transfer behavior and strength. The second objective of this study is also to establish design guidelines and recommendations for composite action when GFRP is used.

### **1.4 Scope**

To assess the performance of the GFRP in the proposed shear transfer application, large scale push-off test specimens were used. Each test specimen consisted of two L-shaped concrete blocks cast at different times. Ten specimens were constructed with an interface shear plane length of 400 mm and ten specimens with 300 mm long shear plane. All specimens were made of 35 MPa concrete. GFRP stirrups having a modulus of elasticity of 50 GPa and GFRP headed bars with a modulus of elasticity of 60 GPa were used to fabricate the specimens. The recorded data includes the longitudinal slip along the

interface plane, the reinforcement strain, and the ultimate strength. The analysis of the test results showed the efficiency of the GFRP as a shear transfer reinforcement. The influence of high GFRP reinforcement content was also determined.

## **1.5 Thesis Organization**

Chapter 2 covers the details of the previous research and literature review associated with the shear transfer in reinforced concrete. The chapter also presents some of the most popular models proposed by different researches and current design codes. Chapter 3 details the experimental program, including a description of the used push-off specimens, materials, preparation, instrumentations and testing. A parametric analysis of the test results is presented in chapter 4. The conclusions and the recommendations are reported in chapter 5.

## **CHAPTER 2**

### **LITERATURE REVIEW**

#### **2.1 Background**

The interfacial shear transfer between the slabs and their supporting beams is of a great importance to the overall load carrying capacity and performance of composite beams. The interfacial shear capacity depends mainly on three parameters, which are the roughness of the interface surface, the amount of reinforcement crossing the interface and the concrete strength. To achieve the desired composite action between the connected members of composite concrete structures, the joints of these members must be able to transfer the longitudinal shear stresses developed along the joints' interfaces. Due to their sensitivity in the design, the evaluation of the capacity and behaviour of concrete joints, such as those of composite concrete beams, were the subject of extensive research.

In the earlier practices of composite construction, the interfacial shear resistance of unreinforced interfaces was thought to be equal to the allowable shear stress of an unreinforced beam (ACI Committee 711, 1953). Therefore, it was assumed that if the interface surface was properly roughened, it could provide an adequate shear strength when combined with shear keys to prevent slippage at the construction joint. An extensive research, regarding the horizontal shear transfer of composite concrete beams was conducted, since 1960. Push-off test specimens, which are the most used in the evaluation of the interface shear were first introduced by Anderson (1960). The first linear shear friction model of the shear transfer was announced by Birkeland and Birkeland (1966). Mast (1968) introduced some refinements to this model and reintroduced a shear friction expression that was later adopted by the ACI 318-70 (1970). A major development of the

shear friction model that lead to the appearance of the modified shear friction hypothesis was done through a series of research by prof. Mattock and his coworkers. The shear friction model and its modified version triggered tremendous interest in this field and many other publications appeared in the literature thereafter. In the vast majority of studies, the shear transfer strength was directly proportional to the amount of steel crossing the concrete joints and linear expressions were proposed. However, other parabolic and non-linear models were also suggested. In all the previous studies, steel reinforcement was the only type of reinforcement used across the concrete joints. The innovative application of Glass Fiber Reinforced Polymer (GFRP) as a shear transfer reinforcement was first investigated by Alkatan (2016). It showed an outstanding performance as compared to steel.

The shear friction was the first and simplest hypothesis to describe the mechanisms by which the shear is transferred along pre-cracked concrete joints. Therefore, it was adopted by most of concrete codes worldwide. According to this theory, under longitudinal shear force (parallel to joint surface), the segment of one side of the joint's crack tend to slip along the crack relative to the other segment on the other side. Upon slipping, the roughness of the crack's interface forces the crack to widen causing tensile stresses in the reinforcement across that crack. This would cause balancing compressive stresses along the crack's faces which leads to resisting longitudinal stresses by the virtue of friction between the sliding faces of the crack (Figure 2.1).

A totally different shear transfer mechanism associated with un-cracked shear planes was first developed by Mattock and Hawkins (1972). For un-cracked concrete joints, the applied shear produces inclined cracks across the shear plane. A truss like action containing the concrete between the cracks as compression struts and the reinforcement placed in the region as tension members is developed (Figure 2.2).

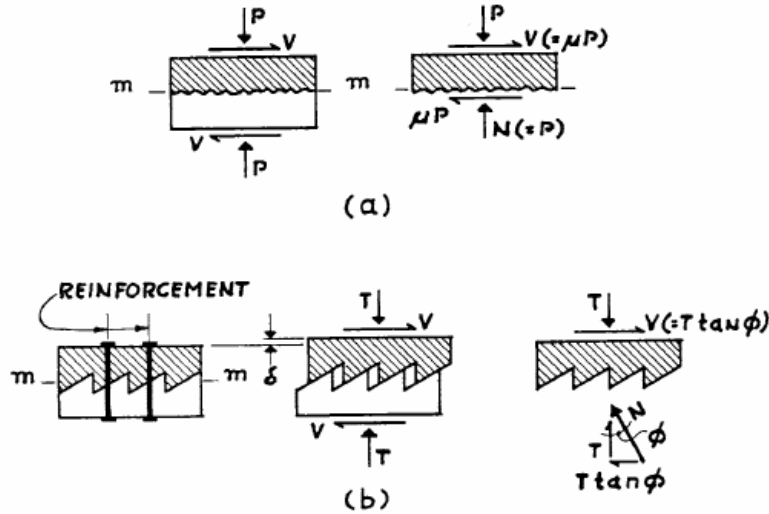


**Figure 2.1** Shear friction hypothesis (Birkeland and Birkeland, 1966)

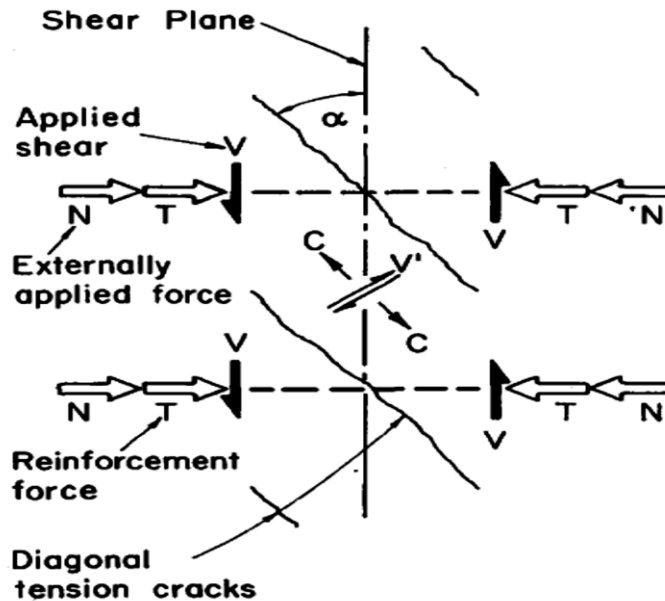


**Figure 2.2** Shear transfer in initially uncracked concrete (Mattock and Hawkins, 1972)



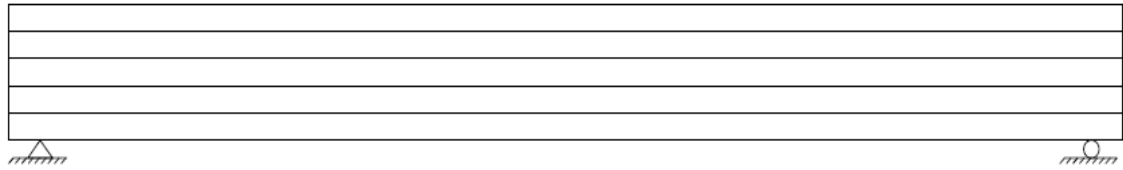
The shear transfer along the concrete joints involves three main mechanisms, which are the adhesion bond, friction, and dowel action (Zilch and Reinecke, 2001). However, a significant dowel action contribution of the reinforcement crossing a concrete joint was shown to be associated with large relative slip beyond what could be acceptable for structural usefulness and, hence, it cannot be considered in the shear transfer design (Paulay et al. 1974).

The concept of longitudinal (horizontal) shear in composite beams is presented in this chapter. A detailed literature review on the subject and related applications are described. Different design parameters as well as the models of the shear transfer proposed by different researchers are stated. The design requirements and expressions adopted by different reinforced concrete codes and standards are discussed.

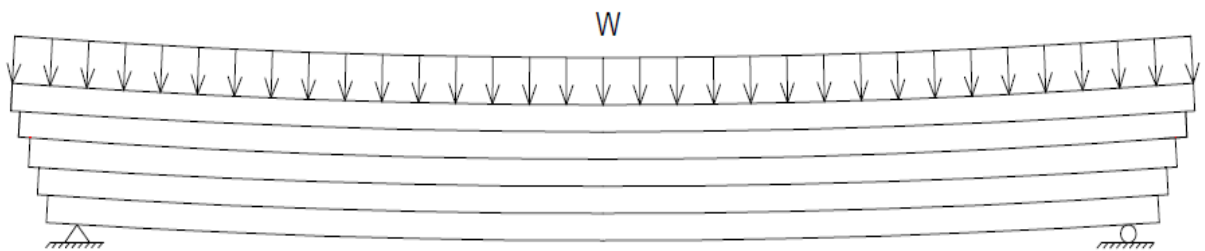
## **2.2 Horizontal Shear in Composite beams**

The existence of horizontal shear stresses in any beam under the action of transverse loads can be verified from Figure 2.3. If a beam is imagined to be made of a series of timbers with smooth interfaces and transverse load,  $w$ , is applied, the planks would then bend independently and each would slide with respect to another, as illustrated in Figure 2.3(b). In this case, no composite action is observed and each piece of timber works as an independent beam having its own compression and tension zone. If the relative sliding between the planks is eliminated by bonding them together, a composite action can be achieved and the strength of the resulted beam would be identical to that of a monolithic beam of similar cross section. While sliding does not occur in the latter case, the tendency to slip still exists under the influence of the horizontal interfacial shear stresses along each

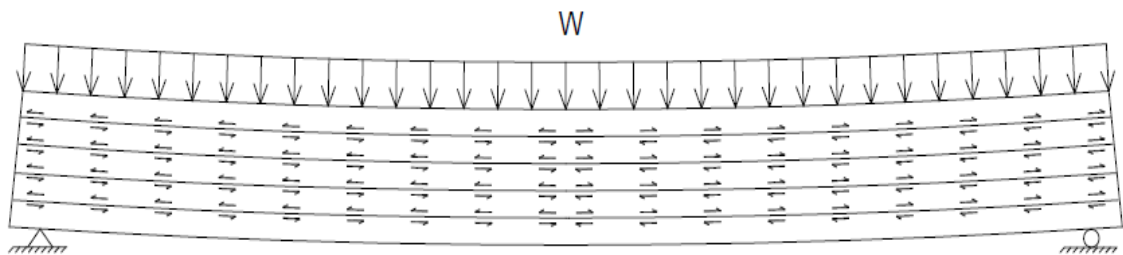
joint. However, these stresses and, hence, the slipping motion is resisted by the adequate bond between the planks [Figure 2.3(c)].



(a) Beam made with multi-planks of timber



(b) Behavior of unbonded planks



(c) Behavior of fully bonded planks

**Figure 2.3** Development of horizontal shear stresses

In a similar manner, to achieve composite action between a precast girder and its cast-in-place flange of a composite concrete beam [Figure 2.4(a)], they need to be perfectly connected through a strong connection that is capable of transferring the horizontal stresses developed under bending along the interface shear plane. Consequently, the composite section can be equivalent to monolithic-cast section with the same geometric properties [Figure 2.4(b)]. If no shear resistance along the joint is achieved and a transversal load is applied, the slab would slip with respect to the beam and no composite action will be attained. In this case, the system will behave as if two separate elements were used, as shown in Figure 2.4(c).

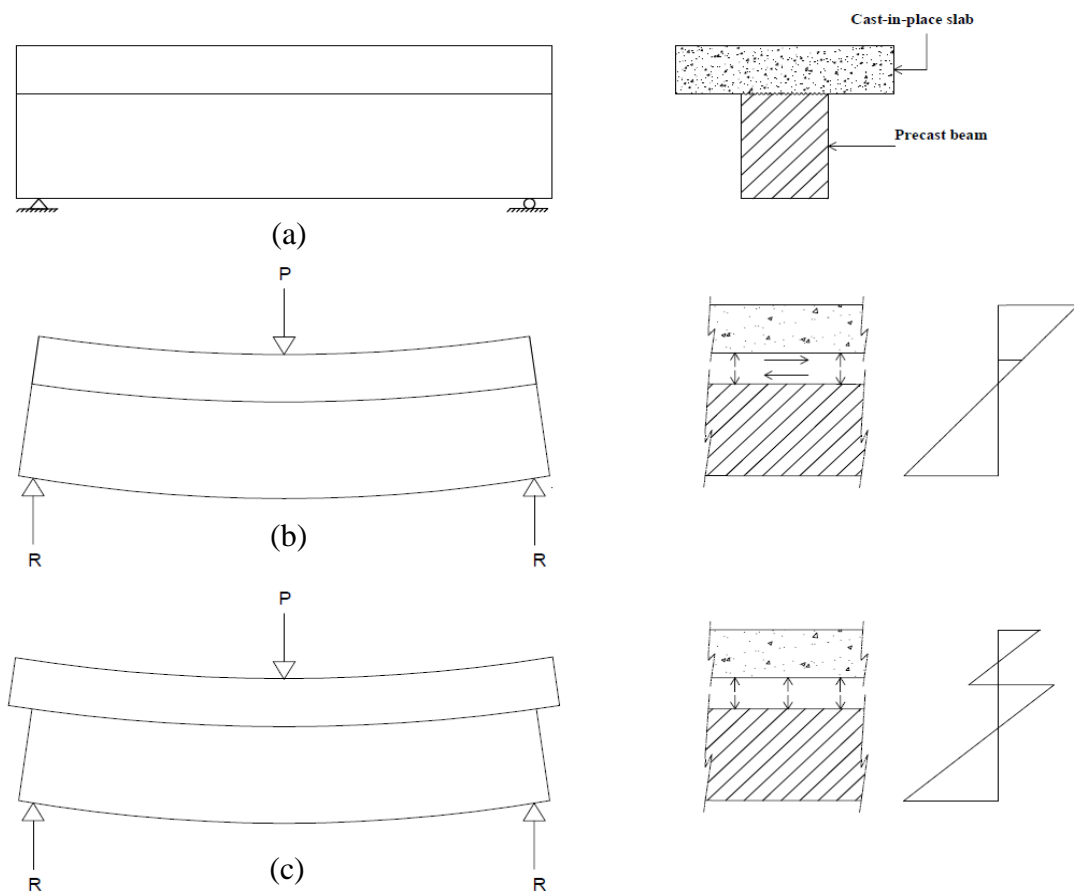


**Figure 2.4** (a) precast beam and cast-in-place slab, (b) composite-section and (c) non-composite section

When a transversal loading is acting on an elastic uncracked beam, the horizontal (longitudinal) shear stresses can be evaluated using the following elastic shear formula (Beer et al. 2014):

$$v_l = \frac{VQ}{Ib} \quad (2.1)$$

where,  $V$  = shear force at the section being studied  
 $Q$  = first moment of the area above or below the contact surface with respect to the natural axis of the section.  
 $I$  = moment of inertia of the entire cross section  
 $b$  = width of the interface between precast and cast-in-place concrete.

The field of application of the elastic formula (Eq. 2.1) may also be extended to elastic cracked sections. However, in this case the cracked properties of the transformed section (i.e. the first and second moment of area) must be used. This formula was also applied in practice and by various researchers to have a rough estimate of the longitudinal stresses in composite concrete beams at the ultimate loads (Loov and Patnaik, 1994; Saemann and Washa, 1964).

As a more reasonable approach to assess the horizontal shear stresses in composite concrete beams, at ultimate loads, both of American and Canadian concrete standards, ACI 318-14 (2014) and CAN/CSA A23.3-14 (2014) specify the horizontal shear stresses to be equal to the vertical (transversal) shear stresses at any given section of the beam. This implies that the horizontal shear stresses at the ultimate load can be calculated using the following expression:

$$v_l = \frac{V_f}{bd} \quad (2.2)$$

where,  $V_f$  is the factored shear force at the section being investigated, and  $d$  is effective depth of the cross section.

In addition to the previous two expressions, the average shear stresses along a segment of the beam can be computed as of the change in the compression force between the two sections of the segment divided by the area of the shear plane between these sections:

$$v_l = \frac{C_f}{bl} \quad (2.3)$$

where  $C_f$  is the total factored compressive force in the cast-in-place flange along the segment under consideration and  $l$  is length of the beam segment under consideration (Figure 2.5).

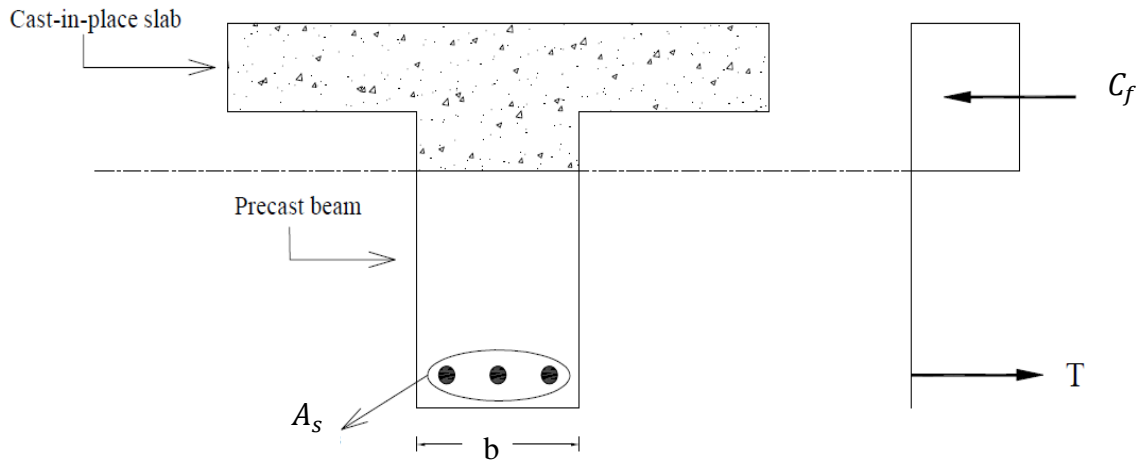


**Figure 2.5** Evaluation of the interface longitudinal shear

### 2.3 Review of Shear Transfer Models

All models describing the shear transfer strength are based mostly on the experimental results of push-off specimens. The parameters of proposed expression were then calibrated to best fit the gathered test data. There are many suggested models to

evaluate the shear transfer strength of the interfaces of concrete joints corresponding to various interface's surface conditions and reinforcement content. These models can be sorted in two categories, namely; 1) linear models and 2) nonlinear models. The most significant models and relative to the present research will be presented for each category separately.

### **2.3.1 Linear Shear Transfer Models**

#### **2.3.1.1 Birkeland and Birkeland, 1966**

In this model, the shear friction theory was proposed for the first time (see Figure 2.1). As mentioned earlier, the interface shear, per this theory, is transferred by the mean of friction generated due to the clamping stress provided by the reinforcement crossing the interface and the friction associated with the roughness of the interface's faces. The authors thought that at the ultimate load the crack width would be large enough to stress the steel across the joint to its yielding limit,  $f_y$ . Accordingly, the first shear friction expression of a concrete-to-concrete interface was in the following from:

$$v_u = \rho_v f_y \mu \quad (2.4)$$

where  $\rho_v$  is the ratio of the reinforcement crossing the interface,  $f_y$  is the yield strength of the steel and  $\mu$  is the coefficient of friction of the interface plane.

Three different values of the coefficient of friction were proposed based on the condition of the concrete joint:

$\mu = 1.7$  for monolithic concrete,

$\mu = 1.4$  for roughened interfaces of concrete joints,

$\mu = 0.8$  to  $1$  for concrete-to-steel joints.

### 2.3.1.2 Mast, 1968

Mast's expression is similar to Eq. 2.4 but he specified a maximum shear transfer strength,  $v_{u,max}$ , of  $0.15f'_c$ . Mast also recommended different values for the coefficient of friction as follows:

- $\mu = 1.4$  to  $1.7$  for a crack in monolithic concrete,
- $\mu = 1.4$  for roughened interfaces of concrete joints,
- $\mu = 1$  for concrete-to-steel joints,
- $\mu = 0.7$  for smooth interfaces of concrete joints.

An important point regarding the shear friction was emphasized that if the steel is to yield at the ultimate, it should be properly anchored on both sides of the shear plane. The coefficient of friction was also considered to be independent of the concrete strength.

### 2.3.1.3 Mattock and Hawkins, 1972

The authors of this study investigated the effect of the shear plane condition (i.e. cracked and uncracked), the clamping stress provided by the reinforcement,  $\rho_v f_y$ , and the external stresses acting parallel and transverse to the shear plane. The findings of this

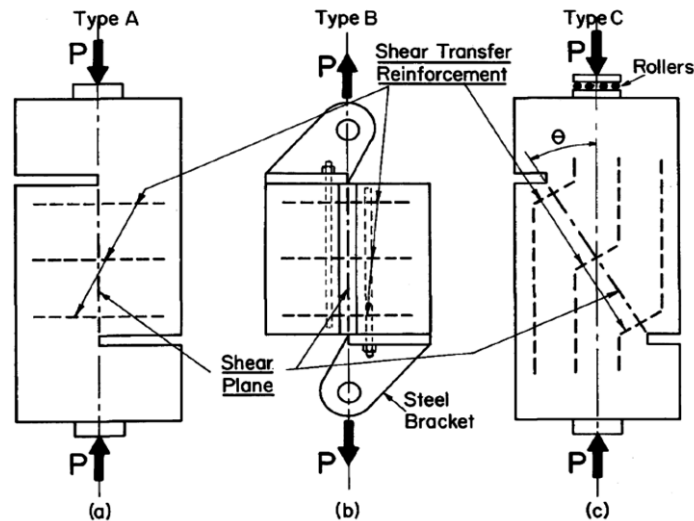


**Figure 2.6** Push-off specimens: (a) Push-off; (b) Pull-off; (c) Modified push-off (Mattock and Hawkins, 1972)

research were based on the experimental results of push-off and modified push-off test specimens shown in Figure 2.6.

Push-off specimens with initially cracked shear planes failed along the existing crack where no diagonal cracks formed across that crack except for the cases where high reinforcement contents were used. The authors suggested that the shear is carried by friction which was considered to be independent of concrete strength. The external clamping stresses provided by external forces, normal to the shear plane, was shown to be effective and could be added to the internal compressive stresses of the reinforcement.

As a lower bound of the test results of initially cracked specimens, the following expression of the ultimate shear transfer resistance was proposed:

$$v_u = 1.38 + 0.8(\rho_v f_y + \sigma_n) \quad \text{in MPa units} \quad (2.5)$$

where  $\rho_v$  and  $f_y$  are the ratio and yield strength of the reinforcement crossing the crack and  $\sigma_n$  is the external clamping stress. An upper limit of the shear strength was introduced as of the least of  $0.3f'_c$  but always less than 10.34 MPa.

Initially uncracked concrete joints with the reinforcement crossing the shear plane at a right angle, behaved in a different manner. Failure was accompanied by the formation of inclined cracks crossing the shear plane. In this case, the transfer of shear was thought to be developed by the truss action (see Figure 2.2).



### 2.3.1.4 Mattock, 1974

This paper presents experimental and analytical study of the shear resistance of concrete shear interfaces inclined at an angle,  $\theta$ , to a parallel or orthogonal array of steel reinforcement (Figure 2.7).

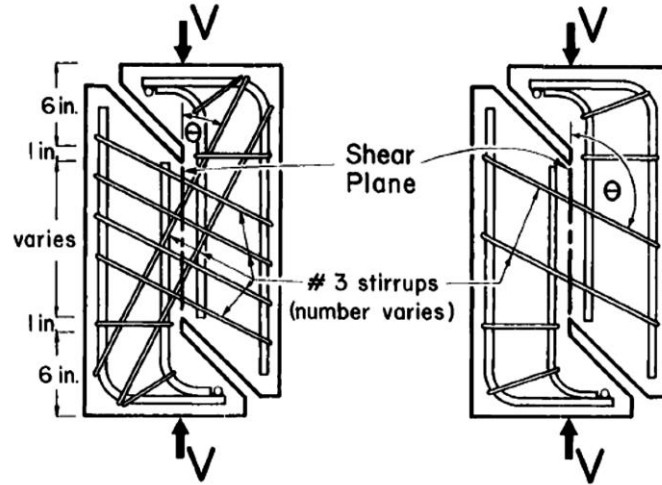


**Figure 2.7** Push-off test specimens with orthogonal and parallel reinforcement (Mattock, 1974)

The following refined version of Eq. 2.5 was proposed. It was based on the mean value of the test results of this study and the previous work of (Mattock and Hawkins, 1972).

$$v_u = 2.76 + 0.8(\rho_v f_y + \sigma_n) \quad \text{in MPa units} \quad (2.6)$$

Equations 2.5 and 2.6 are usually referred to as the modified shear friction equations. They incorporate the interface surface contribution to the shear transfer by cohesion (the first term of Eq. 2.5 and 2.6) and the frictional shear resistance (the second term) which is dependent on the general roughness of the shear plane.

The ultimate shear transfer for parallel reinforcement at an angle  $\theta$  to the shear plane was proposed as follows:

$$v_u = 2.76 \sin^2 \theta + \rho_v f_s (0.8 \sin^2 \theta - 0.5 \sin 2\theta) \quad \text{in MPa units} \quad (2.7)$$

where 0.8 is the coefficient of friction and  $f_s$  is the stress in the reinforcement.  $f_s$  was evaluated as follows:

$$f_s = 0 \text{ for } 0 < \theta < 51.3^\circ$$

$$f_s = -1.6f_y \cos(\theta + 38.7^\circ) \text{ for } 51.3^\circ \leq \theta < 90^\circ$$

$$f_s = f_y \text{ for } 90^\circ \leq \theta \leq 180^\circ$$

### **2.3.1.5 Hermansen and Cowan, 1974**

This work was presented a short paper in which the authors proposed a simple linear expression of the shear transfer. Their model (Eq. 2.8) was prepared based on the test results of reinforced concrete brackets and was found compatible with the test results of Anderson (1960) and Hofbeck et al. (1969) for initially uncracked concrete joints of monolithic construction. The shear transfer capacity was presented as a combination of an apparent cohesion and frictional shear resistance, as follows:

$$v_u = 4.0 + 0.8\rho_v f_y \quad \text{in MPa units} \quad (2.8)$$

### **2.3.1.6 Mattock, Li and Wang, 1976**

The objective of this study was to evaluate the shear transfer strength of concrete joints in precast structures made of lightweight concrete. Initially cracked and uncracked specimens were tested. The diagonal cracks that were reported earlier by Mattock and Hawkins (1972) for cracked specimens with high reinforcement content across their shear plane were not observed here when lightweight concrete was used. For similar concrete strength, interfaces in lightweight concrete was shown to have less shear transfer resistance than those in normal weight concrete.

The authors introduced the following two expressions to calculate the shear transfer capacity of initially cracked interface in lightweight concrete.

For sanded lightweight concrete:

$$v_u = 1.72 + 0.8\rho_v f_y \quad \text{in MPa units} \quad (2.9)$$

provided that  $v_u$  is not greater than  $0.2f'_c$  nor 6.9 MPa and the steel clamping stress,  $\rho_v f_y$ , is higher than 1.38 MPa.

For all-lightweight concrete:

$$v_u = 1.38 + 0.8\rho_v f_y \quad \text{in MPa units} \quad (2.10)$$

provided that  $v_u$  is not greater than  $0.2f'_c$  nor 5.5 MPa and the steel clamping stress,  $\rho_v f_y$ , is higher than 1.38 MPa.

#### **2.3.1.7 Mattock, 1988**

Based on a discussion of a research publication of Walraven et al. 1987, Mattock incorporated the influence of the concrete compressive strength in the cohesion term of Eq. 2.6. The proposed shear resistance was given by the following expression:

$$v_u = 0.467f'_c{}^{0.545} + 0.8(\rho_v f_y + \sigma_n) \quad \text{in MPa units} \quad (2.11)$$

#### **2.3.1.8 Patnaik, 2001**

The behaviour of smooth concrete-to-concrete interfaces between the webs and flanges of composite concrete beams was studied in this research. Push-off specimens were not used here, instead, composite concrete test beams were tested. The reinforcement clamping stress was considered the key factor when it comes to smooth interfaces. A value of the coefficient of friction of 1 was found to best represent the test results. Accordingly, the author recommended the following shear strength for smooth interfaces:

$$v_u = 0.6 + \rho_v f_y \quad \text{in MPa units} \quad (2.12)$$

An upper limit of the shear transfer strength,  $v_u$ , equals to the minimum of  $0.2f'_c$  and 5.52 MPa was proposed. In addition, the reinforcement parameter,  $\rho_v f_y$ , should exceed the minimum of 0.35 MPa. A zero-shear resistance of smooth concrete-to-concrete interfaces with a reinforcement clamping stress,  $\rho_v f_y$ , less than 0.35 MPa was assigned.

### 2.3.1.9 Mattock, 2001

This study represents a comprehensive analysis of the test results of forty-seven initially cracked, along their shear plane, push-off specimens. The objective of this research was to come with unified shear transfer provisions that includes high-strength concrete to improve existing provisions of the ACI 318-99 (1999).

Mattock suggested design expressions for all strengths of concrete. Two expressions were proposed for the shear transfer strength between concrete cast against hardened concrete with an intentionally roughened interface and across a crack in monolithic concrete.

If all the clamping stress, internal by reinforcement and external by external loads, is equal to or higher than  $K_1/1.45$  or if the interfacial shear stress is equal to or greater than  $1.55K_1$ , the shear transfer resistance may be calculated by:

$$v_u = K_1 + 0.8(\rho_v f_y + \sigma_n) \quad (2.13)$$

In this case, the shear transfer resistance is limited to the minimum of  $K_2 f'_c$  and  $K_3$ .

For situations where the total normal stress is less than  $K_1/1.45$  or where the interfacial shear stress is less than  $1.55K_1$ , the shear transfer resistance is proposed as:

$$v_u = 2.25(\rho_v f_y + \sigma_n) \quad (2.14)$$

where, for monolithic normal weight concrete, the coefficient  $K_1$  must not be greater than  $0.1f'_c$  nor 5.52 MPa,  $K_2$  is equal to 0.3 and  $K_3$  is equal to 16.55 MPa. For normal-weight concrete cast against hardened concrete with the substrate surface intentionally roughened,  $K_1$  is equal to 2.76 MPa,  $K_2$  is equal to 0.3 and  $K_3$  is equal to 16.55 MPa. In the case of interfaces of sand-lightweight concrete,  $K_1$  is equal to 1.72 MPa,  $K_2$  is equal to 0.2 and  $K_3$  is equal to 8.27 MPa. For all-lightweight concrete,  $K_1$  is equal to 1.38 MPa,  $K_2$  is equal to 0.2 and  $K_3$  is equal to 8.27 MPa.

Interfaces formed by placing concrete against hardened concrete surface that is not intentionally roughened were assumed to have a shear resistance given by the following expression:

$$v_u = 0.6\lambda\rho_v f_y \quad (2.15)$$

where the maximum shear resistance given by Eq. 2.15 is the lesser of  $0.2f'_c$  and 5.52 MPa.

For concrete cast against unpainted and clean steel and anchored using headed studs or rebars, the ultimate shear transfer strength can be estimated by:

$$v_u = 0.7\lambda\rho_v f_y \quad (2.16)$$

where  $v_u$  should not exceed  $0.2f'_c$  and 5.52 MPa, and  $\lambda$  is equal to 1.00 for normal density concrete, 0.85 for sand-lightweight concrete and 0.75 for all-lightweight concrete.

#### **2.3.1.10 Khan and Mitchell, 2002**

The primary objective of this investigation is to extend the application of the shear friction theory to include high-strength concrete joints. Three different conditions of the shear interfaces were examined; initially uncracked, initially cracked and rough interfaces within concretes cast at different times (cold-joint). Uncracked specimens and those with cold-joint interfaces were observed to have similar ultimate shear transfer capacity. They

also exhibited diagonal cracks crossing the shear plane prior to failure. The authors suggested that the ACI 318-99 (1999) provides a conservative prediction of the shear transfer strength for high-strength concrete and they suggested the following expression for rough and uncracked interface:

$$v_u = 0.05f'_c + 1.4\rho_v f_y \quad (2.17)$$

The proposed maximum shear transfer resistance,  $v_u$ , is equal to  $0.2f'_c$ . The used steel in this study had a yield strength of 479 MPa.

#### **2.3.1.11 Harries, Zeno and Shahrooz, 2012**

The validity of a primary assumption the shear friction that steel, crossing a concrete joint, yields at ultimate was examined. Only eight push-off test specimens were tested. The interfaces of these specimens were produced by casting the concrete of one part of each specimen against the hardened concrete of the second one (cold-joint).

The main finding of this study was that the high-grade steel reinforcement that was used across the shear plane did not yield and the stress was well below its yield point. Therefore, the authors recommend that the internal clamping stress provided by the steel reinforcement should be treated as a function to the reinforcement stiffness, rather than its yield strength. Consequently, the following formula was recommended:

$$v_u = \alpha f'_c + 0.002E_s \rho_v \quad (2.18)$$

where the maximum shear transfer strength is proposed as  $0.2f'_c$ ,  $E_s$  is the steel modulus of elasticity. The coefficient  $\alpha$  was determined as follows;  $\alpha = 0.075$  for monolithic concrete,  $\alpha = 0.040$  for cold-joint interfaces and  $\alpha = 0$  for initially cracked interfaces.

### 2.3.1.12 Alkatan, 2016

The innovative application of the Glass Fiber Reinforced Polymer (GFRP) as a shear transfer reinforcement across interfaces between concretes cast at different times was first examined in Alkatan's thesis. Large scale Push-off test specimens were constructed and used. Three different shapes of GFRP reinforcement were used, namely; a) stirrups; b) headed bars and c) bent bars (angles). In addition, an intermediate grade GFRP with a modulus of elasticity of 50 GPa (stirrups and bent bars) and high modulus GFRP with a modulus of 60 GPa (headed bars) were examined.

The nominal ultimate shear transfer resistance was found to correspond to a maximum strain of 5000 microstrain in GFRP reinforcement. For a lower bound formulation of the test results, the cohesion contribution was suggested to be equal to  $0.04f'_c$ . The suggested coefficient of friction ( $\mu$ ) of the cold-joint interfaces of the test specimens was determined as 1. Accordingly, the proposed shear transfer expression was in the following form:

$$v_u = 0.04f'_c + \varepsilon_F E_F \rho_v \sin \alpha_f + \varepsilon_F E_F \rho_v \cos \alpha_f \quad (2.19)$$

where,  $0.04f'_c + \varepsilon_F E_F \rho_v \sin \alpha_f \leq 0.25f'_c$ ,  $f'_c$  is the concrete compressive strength,  $\varepsilon_F$  is the strain in the GFRP reinforcement at the ultimate load ( $\varepsilon_F = 0.005$ ),  $E_F$  is the modulus of elasticity of the used FRP reinforcement,  $\rho_v$  is the reinforcement ratio and  $\alpha_f$  is the angle of inclination of the reinforcement with respect to the shear plane.

A minimum reinforcement parameter,  $E_F \rho_v$ , of  $203 \text{ N/mm}^2$  was discovered to be mandatory in order to activate the role of the GFRP reinforcement in the shear transfer. Below this value the interfaces were found to have a shear resistance close to that of an unreinforced concrete interface with similar concrete compressive strength.

## 2.3.2 Nonlinear Shear Transfer Models

### 2.3.2.1 Birkeland, 1968

Based on the gathered test data available at the time, Birkeland (1968) was the first researcher to propose the following nonlinear expression to predict the ultimate shear transfer resistance.

$$v_u = 2.78 \sqrt{\rho_v f_y} \quad \text{in MPa units} \quad (2.20)$$

This expression did not get the attention the linear shear friction expression received. It does not have the simplicity and the physical impact provided by the shear friction.

### 2.3.2.2 Raths, 1977

In this publication, a nonlinear shear transfer model similar to Eq. 2.20 (Birkeland, 1968) was suggested. The main difference was the inclusion of the concrete density as follows:

For interfaces in monolithic concrete:

$$v_u = 3.11 C_s \sqrt{\rho_v f_y} \quad \text{in MPa units} \quad (2.21)$$

For smooth interfaces:

$$v_u = 2.03 C_s \sqrt{\rho_v f_y} \quad \text{in MPa units} \quad (2.22)$$

where  $C_s$  represents the influence of the concrete density. Three different values of  $C_s$  were recommended; a) 1.00 for normal-weight concrete; b) 0.85 for sand-lightweight concrete and c) 0.75 for all-light weight concrete.



### 2.3.2.3 Loov, 1978

Loov (1978), cited by Loov and Patnaik (1994), introduced the first expression that considers concrete strength,  $f'_c$ , in the evaluation of the shear transfer. Being the ultimate shear transfer resistance given by:

$$v_u = k\sqrt{\sigma f'_c} \quad (2.23)$$

where  $k$  is equal to 0.5 for initially uncracked interfaces,  $\sigma = \sigma_n + \rho_v f_y$  is the total compressive stress across the shear plane and  $\sigma_n$  is the clamping stress provided by the external forces normal to the shear plane.

### 2.3.2.4 Walraven, Frénay and Pruijssers, 1987

An extensive statistical analysis of eighty-eight push-off test specimens was conducted. The focus in this analysis was the concrete strength because the authors were convinced that it has an influence on the shear transfer and its absence from most of the previous models, particularly shear friction, was due to the fact that the used test specimens were constructed using a concrete strength varying in a narrow range of 20 to 30 MPa, which may have masked the influence of the concrete strength by the natural scatter of the experimental results. The proposed design expressions were as follows:

$$v_u = C_1 (\rho_v f_y)^{C_2} \quad \text{in MPa units} \quad (2.24)$$

where  $C_1 = 0.822 f'_{cc}{}^{0.406}$ ,  $C_2 = 0.159 f'_{cc}{}^{0.303}$ ,  $f'_{cc}$  is the concrete compressive strength of 150 mm (5.9 in) cubes ( $f'_c = 0.85 f'_{cc}$ );  $\rho_v$  is the reinforcement ratio and  $f_y$  is the yield strength of the steel. The authors realized the complexity of their equation. Therefore, a design chart to represent Eq. 2.24 was prepared to simplify the design process.

### 2.3.2.5 Mau and Hsu, 1988

In their discussion of the study of Walraven et al. (1987), the authors suggested that the web reinforcement index ( $\rho_v f_y / f'_c$ ) was the dominant factor in determining of the shear transfer strength. Based on a statistical analysis, the proposed design expression was given in the following non-dimensional form:

$$\frac{v_u}{f'_c} = 0.66 \sqrt{\frac{\rho_v f_y}{f'_c}} \quad (2.25)$$

provided that  $v_u / f'_c < 0.3$

This equation is similar to Loov's equation (Eq. 2.23). However, a constant of 0.66 was suggested for both initially cracked and uncracked interfaces. This assumption is questionable since the behaviour of initially cracked specimens was shown to be quite different from that of initially uncracked specimens (Mattock and Hawkins, 1972; Mattock et al. 1976).

### 2.3.2.6 Loov and Patnaik, 1994

The work of Loov and Patnaik (1999) was an experimental study of sixteen composite concrete beams with beam-slab cold-joint interfaces. The beams substrate surfaces were left natural (as-cast) and no further treatment was done prior to the application of the flange. The ultimate load was considered to have occurred when the relative slip along the shear plane reached, at least, 0.5 mm. At this value of slip, the reinforcement across the joint was reported to have yielded.

The authors recommend a modified version of Loov's nonlinear equation (Eq. 2.23) as follows:

$$v_u = \lambda k \sqrt{(0.1 + \rho_v f_y) f'_c} \quad \text{in MPa units} \quad (2.26)$$

where  $\lambda$  is a factor to account for the concrete density;  $\lambda = 1$  for normal-weight concrete;  $\lambda = 0.85$  for sand-lightweight concrete and  $\lambda = 0.75$  for all-lightweight concrete. The constant  $k$  was empirically found to be equal to 0.6. Yet, to allow for possible variation in the as-cast roughness of the interfaces in practical applications, the value of  $k$  of 0.5 was recommend for composite construction. The ultimate shear resistance was limited to the maximum of  $0.25f'_c$ .

### 2.3.2.7 Mattock, 1994

Mattock (1994) commented on previous paper (Loov and Patnaik, 1994) where he suggested that the nominal shear is not proportional to  $\sqrt{f'_c}$  as implied by Eq. 2.26, Instead, Mattock proposed a design expression as a lower bound of the test results of Loov and Patnaik (1994). Being the ultimate design shear stress for a crack in monolithic normal-weight concrete, predicted by:

$$v_u = \frac{\sqrt{\rho_v f_y}}{4.536} f_c^{0.73} \quad \text{in MPa units} \quad (2.27)$$

where the value of the shear transfer stress resistance,  $v_u$ , is limited to  $0.3f'_c$ .

The shear transfer strength of initially cracked interfaces between concretes cast-at-different times was found to be  $0.02f'_c$  less than that of cracked interfaces in monolithic concrete given by Eq. 2.27. Accordingly, the author suggested the following expression for cracked and roughened cold-joint interfaces:

$$v_u = \frac{\sqrt{\rho_v f_y}}{4.536} f_c^{0.73} - 0.02f'_c \quad \text{in MPa units} \quad (2.28)$$

It was also pointed out that the interface roughness plays a major role in the shear transfer strength. Therefore, quantifying the roughness were recommended to be continued to be specified in the ACI code to ensure adequate interface roughness in practice.

#### **2.3.2.8 Ali and White, 1999**

Based on the contact density model developed by Li and Maekawa (1987) which describes the contact surface and its behaviour, the authors proposed an analytic procedure to predict the shear transfer strength of the concrete joints. In their analysis, the following essential parameters were examined: (1) concrete strength; (2) shear reinforcement across the interface; (3) normal stress at the interface; (4) roughness of interface surface. The proposed ultimate shear transfer strength expression is as follows:

$$\frac{v_u}{f'_c} = 1.47a \sqrt{\frac{\rho_v f_y + \sigma_n}{f'_c}} \quad (2.29)$$

where  $v_u$  is the ultimate shear stress,  $\rho_v$  is the reinforcement ratio,  $f_y$  is the yield strength of the steel reinforcement,  $\sigma_n$  is the external normal to the shear plane stress. The shear resistance was upper limited to a value of  $1.4b$ .  $a$  and  $b$  are empirical parameters related to the concrete density.

Virtually, this equation is similar to the model recommended by Mau and Hsu (1988) (Eq. 2.25). However, Eq. 2.29 was derived from purely analytical procedure.

#### **2.3.2.9 Mansur, Vinayagam and Tan, 2008**

Both analytical and experimental investigation were carried on in (Mansur et al., 2008). This research initiative was to study the behaviour of cracked concrete interfaces. An examination and comparison between previous proposed design expressions for high

strength concrete, up to 100 MPa, were made. The test matrix of this study consisted of nineteen push-off test specimens. All specimens had their shear plane precracked prior to the application of shear load. The test parameters included the concrete strength and the reinforcement content.

Similar to the expression provided by Mau and Hsu (1988) (Eq. 2.25), the authors suggested the following formula:

$$\frac{v_u}{f'_c} = 0.566 \left( \frac{\rho_v f_y}{f'_c} \right)^{0.5} \quad (2.30)$$

where  $v_u$  is to be taken higher than  $0.3f'_c$ .

A trilinear formulation for the shear transfer was also proposed as follows:

For normalized clamping stress,  $\rho_v f_y / f'_c \leq 0.075$ :

$$\frac{v_u}{f'_c} = 2.5 \left( \frac{\rho_v f_y}{f'_c} \right) \quad (2.31)$$

For  $0.075 < \rho_v f_y / f'_c < 0.270$ :

$$\frac{v_u}{f'_c} = \frac{0.56}{(f'_c)^{0.385}} + 0.55 \left( \frac{\rho_v f_y}{f'_c} \right) \quad \text{in MPa units} \quad (2.32)$$

and for  $\rho_v f_y / f'_c \geq 0.270$ :

$$\frac{v_u}{f'_c} = 0.3 \quad (2.33)$$

## 2.4 Shear Transfer Provisions in existing Design Codes and Standards

Shear transfer provisions in common north American codes and standards are presented in the following. The expressions of the nominal shear transfer strength provided by each standard are also indicated.

#### 2.4.1 AASHTO Standard Specifications for Highway Bridges, 2002

The shear transfer strength along an existing or possible crack along reinforcement concrete sections is predict based on the shear friction theory (Birkeland and Birkeland, 1966).

$$v_u = \rho_v f_y (\mu \sin \alpha_f + \cos \alpha_f) \quad (2.34)$$

Provided that  $v_u$  is not grater than  $0.09f'_c$  nor 2.5 MPa. Various values of the friction coefficient,  $\mu$ , are specified for different conditions of the substrate surface. For potential cracks in monolithic concrete,  $\mu$  is equal to  $1.4\lambda$ ; for situations where the concrete is placed against a roughened substrate surface to an average amplitude of 6.35 mm,  $\mu$  is equal to  $1.0\lambda$ ; if the substrate surface is not intentionally roughened,  $\mu$  is equal to  $0.6\lambda$ ; lastly, for concrete-to-steel joint,  $\mu$  is equal to  $0.7\lambda$ . where  $\lambda$  is the concrete density factor taken as 1.00 for normal-weight concrete, 0.85 for sand-lightweight concrete and 0.75 for all-lightweight concrete. For composite concrete beams, at their joint, a minimum reinforcement ratio,  $\rho_v$ , of  $50/f_y$  (psi units) is suggested by this standard.

#### 2.4.2 Canadian Design Code of Concrete Structures, CAN/CSA A23.3, 2014

This code provides two expressions to calculate the nominal shear transfer capacity of the concrete-to-concrete interface. The first one is adopted from the modified shear friction theory initially proposed by Mattock and Hawkins (1972) and Mattock (1974).

$$v_u = \lambda(c + \mu\sigma) + \rho_v f_y \cos \alpha_f \quad (2.35)$$

Provided that the first term,  $\lambda(c + \mu\sigma)$ , is not greater than  $0.25f'_c$ . the concrete density factor is specified as follows;  $\lambda = 1.00$  for normal desnity concrete;  $\lambda = 0.85$  for semi-low density concrete; and  $0.75$  for low density concrete. The cohesion stress,  $c$  and the frction coefficient  $\mu$  are suggested as follows; for concrete placed against not roughened

hardened concrete,  $c = 0.25$  and  $\mu = 0.6$ ; for concrete placed against hardened concrete with the substrate surface intentionally roughened to a minimum of 5 mm amplitude,  $c = 0.50$  and  $\mu = 1.00$ ; for monolithic construction,  $c = 1.00$  and  $\mu = 1.4$ ; and for concrete-to-steel connections,  $c = 0$  and  $\mu = 0.60$ .

The design expression proposed by Loov and Patnaik (1994) was adopted to evaluate the shear transfer resistance of rough interface, in addition to the shear friction theory.

$$v_u = \lambda k \sqrt{\sigma f'_c} + \rho_v f_y \cos \alpha_f \quad (2.36)$$

The first term of this equation is limited to the value of  $0.25f'_c$ . the constant  $k$  was chosen as 0.5 for composite construction and 0.6 for monolithic construction. This code also specifies a minimum ratio of steel reinforcement across concrete joints of  $0.06\sqrt{f'_c}/f_y$ .

#### **2.4.3 Canadian Bridge and Highway Design Code, CAN/CSA S6, 2014**

The modified shear friction expression specified in CAN/CSA A23.3 (2014) (Eq. 2.35) is also used in this standard. However, there is no indication of situations where the shear transfer reinforcement is inclined to the shear plane and, hence, the second term of Eq. 2.35 is not included in the S6-14 shear transfer provision. In addition to the limit of  $0.25f'_c$ , the bridge code imposes another maximum limit of 6.5 MPa for the term  $(c + \mu\sigma)$ . A summary of the shear transfer provision of this code is shown in Table 2.1.

#### **2.4.4 American Concrete Institute Code Requirements for Structural Concrete, ACI 318, 2014**

Soon after the shear friction theory was proposed, the American standard ACI 318 adopted it to predict the shear transfer strength of concrete interfaces such as those found in composite construction. The nominal frictional shear resistance specified in this code is as follows:

$$v_u = \rho_v f_y (\mu \sin \alpha_f + \cos \alpha_f) \quad (2.37)$$

The coefficient of friction in this expression is quantified for various states of the interface substrate surface. For monolithic concrete,  $\mu = 1.4\lambda$ ; for concrete placed on hardened and roughened to 6.35 mm amplitude,  $\mu = 1.0\lambda$ ; for concrete interface that is not roughened,  $\mu = 0.6\lambda$ ; for concrete against steel surfaces,  $\mu = 0.7\lambda$ . The concrete density modification factor,  $\lambda$ , is specified as follows; 1.00 for normal-weight concrete; and 0.75 for all lightweight concrete.

Table 2.1 summarizes the design code requirements discussed in this section. The limitations and parameters associated with each standard are stated as well.



**Table 2.1** Shear transfer Design Expressions

Design Standard	Nominal Shear Transfer Strength	Parameters/Limits
AASHTO (2002)	$v_u = \rho_v f_y (\mu \sin \alpha_f + \cos \alpha_f)$	$\mu = 1.4 \lambda$ for monolithic concrete. $\mu = 1.0 \lambda$ for artificially roughened surfaces to 6.35 mm. $\mu = 0.6 \lambda$ for not intentionally roughened interfaces. $\mu = 0.7 \lambda$ for concrete anchored to steel surface. $\lambda = 1$ for normal-weight concrete. $\lambda = 0.85$ for sand-lightweight concrete $\lambda = 0.75$ for all-lightweight concrete. $\rho_{v,min} = 50/f_y$ (psi units)
CAN/CSA A23.3 (2014)	$v_u = \lambda(c + \mu\sigma) + \rho_v f_y \cos \alpha_f$	$c = 1; \mu = 1.4$ for monolithic concrete. $c = 0.5; \mu = 1$ for intentionally roughened surfaces to a minimum of 5mm. $c = 0.25; \mu = 0.6$ for not intentionally roughened interfaces. $c = 0; \mu = 0.6$ for concrete-to-steel joints. $\lambda = 1$ for normal density concrete; $\lambda = 0.85$ for semi-low-density concrete; and $\lambda = 0.75$ for low-density concrete $\lambda(c + \mu\sigma) \leq 0.25 f'_c$ $\rho_{v,min} = 0.06 \sqrt{f'_c} / f_y$
	$v_u = \lambda k \sqrt{\sigma f'_c} + \rho_v f_y \cos \alpha_f$	$\lambda k \sqrt{\sigma f'_c} \leq 0.25 f'_c$ $k = 0.5$ for concrete placed against hardened concrete. $k = 0.6$ for concrete placed monolithically.
CAN/CSA S6 (2014)	$v_u = (c + \mu\sigma)$	$c = 1; \mu = 1.4 \lambda$ for monolithic concrete. $c = 0.5; \mu = 1 \lambda$ for intentionally roughened surfaces to a minimum of 5mm@15 mm spacing. $c = 0.25; \mu = 0.6 \lambda$ for not intentionally roughened interfaces. $\lambda = 1$ for normal-density concrete; $\lambda = 0.85$ for semi-low-density concrete; and $\lambda = 0.75$ for low-density concrete $(c + \mu\sigma) \leq 0.25 f'_c$ and 6.5 MPa.
ACI 318 (2014)	$v_u = \rho_v f_y (\mu \sin \alpha_f + \cos \alpha_f)$	$\mu = 1.4 \lambda$ for monolithic concrete. $\mu = 1.0 \lambda$ for artificially roughened surfaces to 6.35 mm. $\mu = 0.6 \lambda$ for not intentionally roughened interfaces. $\mu = 0.7 \lambda$ for concrete anchored to steel surface. $\lambda = 1$ for normal-weight concrete. $\lambda = 0.75$ for all-lightweight concrete. $\rho_{v,min} = \text{greater of } 0.75 \sqrt{f'_c} / f_y \text{ and } 50 / f_y \text{ (psi units)}$

## 2.5 Summary

The review of the literature of shear transfer mechanism has been summarized in this chapter. Different shear transfer models of concrete joints proposed have also been presented. The design requirements of some major design codes and standards have been illustrated. It is established that the design for longitudinal shear along concrete-to-concrete interfaces in the concrete codes was mainly based on the shear friction theory and its modified version. This theory has a simple linear expression and presents the designer with a visual and physical impact of the shear transfer mechanism, which is not the case of nonlinear shear transfer expressions. However, it has to be highlighted that all of the developed models discussed in the proceeding chapter were empirically calibrated to fit the experimental results of push-off specimens. The key parameters of the shear friction theory are the condition and preparation of the interface surface and the reinforcement parameter ( $\rho_v f_y$ ). The cohesion term was later introduced to the shear friction theory to account for the cohesion contribution of the concrete surface to the shear transfer. This term was modified afterward and considered to be a function of the concrete compressive strength (Mattock and Hawkins, 1972; Mattock 1974; Mattock 1988; Khan and Mitchell, 2002; Patnaik 2001; Alkatan, 2016). Generally, the transfer of shear was shown to involve three sub-transfer mechanisms, which are cohesion, friction and dowel action. However, a significant dowel action contribution to the shear transfer was associated with high slip along the joints (paulay et al. 1974).

The performance of Glass Fiber Reinforced Polymer (GFRP) as shear transfer reinforcement was first studied by Alkatan (2016). It was found to be effective and compatible to steel reinforcement. Furthermore, in this particular application, the ability of

the GFRP to deform much further was found to provide an outstanding ductile failure mode with a significant residual strength post to the cracking of the shear plane.

## **CHAPTER 3**

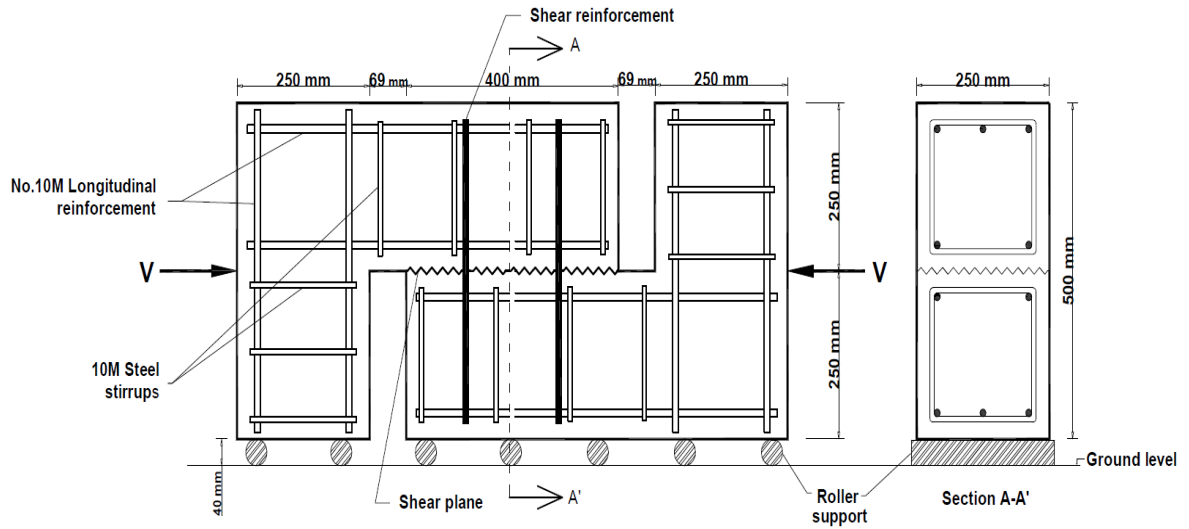
### **EXPERIMENTAL PROGRAM**

#### **3.1 Introduction**

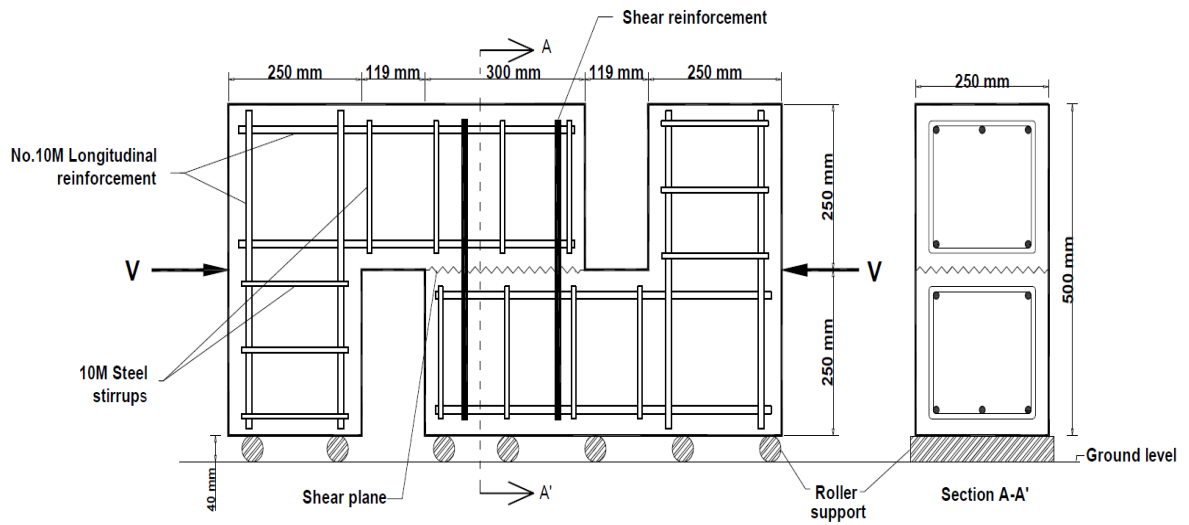
The present research objective is to extend the investigation conducted by (Alkatan, 2016). Alkatan conducted a series of push-off tests to illustrate the advantage of using GFRP reinforcement for concrete shear connection. The push-off test is commonly used for studying shear transfer mechanisms. It was developed by Anderson (1960) to study the shear-slip behavior of concrete joints connecting precast concrete girders and cast in place slabs. Alkatan (2016) research covered a limited range of reinforcement ratio. The present investigation extends the range of reinforcement ratio by reducing the interface surface and increasing the amount of reinforcement. The surfaces of the concrete joints of the proposed specimens were not treated, roughened or smoothened. Instead, they were left as-cast. Two types of GFRP reinforcement were used, which are stirrups and headed bars. The used concrete had an average compressive strength of about 35 MPa for all tested specimens. The specimens were tested in a horizontal position as it is found to be easier to conduct. LVDTs and strain gauges were used to measure the slip along the shear interface and the strain in the reinforcement crossing the interface. The test specimens were divided into two series according to the dimensions of the shear plane. The first Series (A1) includes specimens with a shear plane of dimensions of 250 x 400 mm and the second series (A2) are specimens with shear plane of dimensions of 250 x 300 mm. The present chapter gives, the details of the test matrix, test specimens, fabrication and the test setup.

### 3.2 Test Specimens

The experimental program of the current research consists of testing twenty push-off specimens. Each specimen, was cast horizontally in two stages. For each specimen, seven days after casting the first L-shaped concrete block (half), the second block was cast on top of it. This resulted in a cold-joint condition along the interface between the two concrete blocks, as can be seen in Figures 3.1(a) and 3.1(b). The shear plane, which is the interface surface between the connected L-shaped concrete blocks was 250 mm wide. The shear plane was 400 mm long in the ten specimens of series A1. Whereas, in ten others, the shear plane length was limited to 300 mm to allow for further variation in the reinforcement ratio. All of series A1 specimens had a shear plane area of  $100000 \text{ mm}^2$ , while the shear plane area of series A2 specimens was  $75000 \text{ mm}^2$ . The overall depth of the specimen was 500 mm and its total length was about 1040 mm. The gaps between the connected blocks at both ends of the shear plane were left to allow for a relative slip once the shear load is applied. Figure 3.1(a) shows the typical design configuration of the test push-off specimen with 400 mm long shear plane. The typical design configuration of push-off specimen with 300 mm long shear plane is shown in figure 3.1(b). Figures 3.1(a) and 3.1(b) also shows the shear transfer reinforcement placement across the shear plane.



(a) Design configuration of push-off specimens with 400 mm shear plane length



(b) Design configuration of push-off specimens with 300 mm shear plane length

**Figure 3.1** Design configuration of push-off specimens

GFRP stirrups and head bars (Figure 3.2) were used as shear transfer reinforcement. Three GFRP-stirrup reinforced specimens, five with GFRP headed bars, one with two steel stirrups and one with no reinforcement were used in each of series A1 and A2 of this study. The average compressive strength of the corresponding concrete cylinders for all specimens was about 35 MPa. The variable parameters among these specimens were the reinforcement stiffness parameter ( $E\rho_v$ ) and the GFRP reinforcement shape (stirrups and headed bars). Specimens of series A2 are designed with smaller interface surface compared to series (A1) to allow the extension of the reinforcement ratio range.

The test matrix of the current study is illustrated in Table 3.1. The specimens are named so that the first letter indicates the type of the shear transfer reinforcement used across the shear plane; F for GFRP and S for steel. The second letter points out to the shape of this reinforcement; S for stirrups and H for headed bars. The number following the letters represents the number of stirrups or headed bars used in each specimen. Reference to series 1 and 2 are made by A1 and A2, respectively. For instance, FH4-A1 is the push-off specimen of series A1 utilizing four GFRP headed bars across its shear plane. To evaluate the contribution of the concrete interface alone, two specimens C0-A1 and C0-A2 with no reinforcement were used. Furthermore, the steel reinforced specimens SS2-A1 and SS2-A2 were intended to be used for comparison with that of GFRP reinforced specimens.

The concrete blocks for all specimens were made of ready mix concrete with an average compressive strength of about 35 MPa concrete. The modulus of elasticity of GFRP stirrups was 50 GPa, whereas it was 60 GPa for headed bars according to the supplier information (VROD – Canada). The variation of the reinforcement ratio by changing the area of the contact surface between series A1 and A2 along with using two different

stiffness of GFRP (50 and 60 GPa) resulted in the variation of reinforcement stiffness parameter ( $E\rho_v$ ) between 228 and 811 MPa for GFRP reinforced specimens. To avoid bending moments and shear stresses other than the shear along the interface plane, the specimens were loaded with a hydraulic jack as shown in Figures 3.1(a) and 3.1(b).



**Figure 3.2** Shapes of GFRP reinforcement



**Table 3.1** Test matrix

Specimen	Reinforcement type and shape	$A_v$ ( $mm^2$ )	$A_{cv}$ ( $mm^2$ )	$\rho_v$ (%)	$E$ (GPa)	$E\rho_v$ (MPa)
C0-A1	NA	0.0	100000 (250x400)	0.00	0.0	0.0
SS2-A1	Steel stirrup	400.0		0.40	200	800
FS2-A1	GFRP stirrup	506.8		0.51	50	253
FS3-A1		760.2		0.76		380
FS4-A1		1013.6		1.01		507
FH3-A1	GFRP headed bar	380.1		0.38	60	228
FH4-A1		506.8		0.51		304
FH5-A1		633.5		0.63		380
FH6-A1		760.2		0.76		456
FH8-A1		1013.6		1.01		608
C0-A2	NA	0.0	75000 (250x300)	0.00	0.0	0.0
SS2-A2	Steel stirrup	400.0		0.53	200	1067
FS2-A2	GFRP stirrup	506.8		0.68	50	338
FS3-A2		760.2		1.01		507
FS4-A2		1013.6		1.35		676
FH3-A2	GFRP headed bar	380.1		0.51	60	304
FH4-A2		506.8		0.68		405
FH5-A2		633.5		0.84		507
FH6-A2		760.2		1.01		608
FH8-A2		1013.6		1.35		811

### 3.3 Fabrication of the Push-off Specimens

To cast the push-off specimens five wooden formworks were built. The formworks were constructed in a way that allows for the two blocks of each specimen to be cast at different times and form what is cold-joint conditions along the interface surface of the specimens. Figure 3.3 shows the used wooden formworks. The formwork was constructed

using three-quarters inch thick laminated plywood sheets. The plywood sheets were supported by wooden beams to prevent lateral deformation of the formworks during casting (see Figure 3.3).



**Figure 3.3** Wooden Formworks

After the formworks were built, the strengthening steel reinforcement in the form of 10M bars and stirrups were used to prevent local failures and guarantee a shear transfer failure along the interface of the push-off specimen. The stirrups and bars were tied up together prior to installation in the formwork which resulted in two steel cages; one along

the specimen's web (horizontal portion) and another along the specimen's flange (vertical portion), as shown in Figure 3.4.



**Figure 3.4** Steel cages

Subsequently, the reinforcement was secured in its place in the formwork using plastic chairs to maintain them one inch of concrete cover all around the perimeter of the formwork interior surfaces. Figure 3.5 illustrates the strengthening steel reinforcement placed in its position. The shear transfer reinforcement assigned for each specimen was firmly tied and secured to the steel cages allowing for sufficient anchorage on both sides of the specimen (see Figure 3.6). The wooden formwork was sprayed with oil to prevent sticking of the hardened concrete, and facilitate the disassembly of the formwork.



**Figure 3.5** Steel cages installed for the first halves of 4 specimens before concrete casting



**Figure 3.6** Shear transfer reinforcement secured to the steel cages of first specimen's halves before concrete casting



All specimens were cast horizontally at once in two stages. The first halves of the specimens were cast first. Concrete was added and vibrated in layers to obtain a uniform casting throughout. The top surface was left natural (as-cast) with no further treatment. Figure 3.7 shows the cast halves of four specimens. Next, the fresh concrete in the formworks was covered by a wet burlap. A plastic sheet was also used on top of the burlap wrapping all specimens. The first halves were kept wet for curing for seven days, after which the loose concrete particles and dust were removed from the top surfaces.

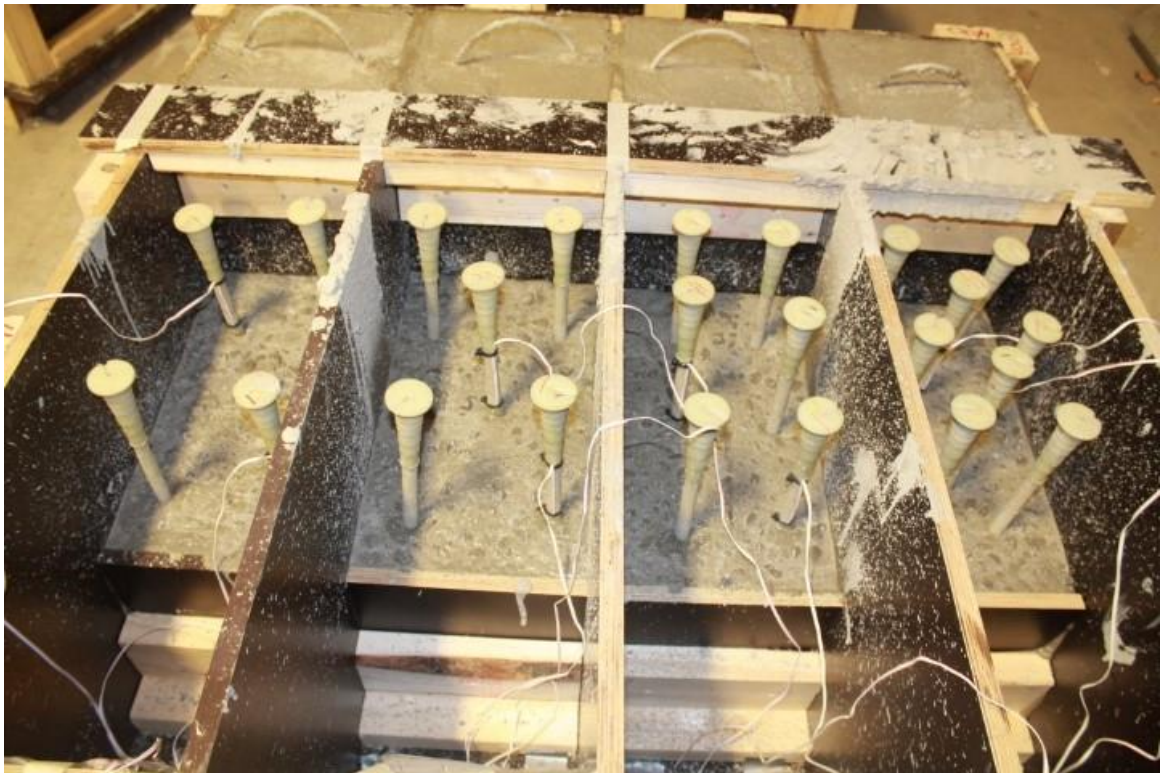


**Figure 3.7** Cast of first blocks and the shear reinforcement is extended from the top surfaces prior to casting second specimen's blocks

The steel cages associated with second block of each specimen were then installed and held in place (see Figure 3.8). Plastic reinforcement chairs were also used herein to



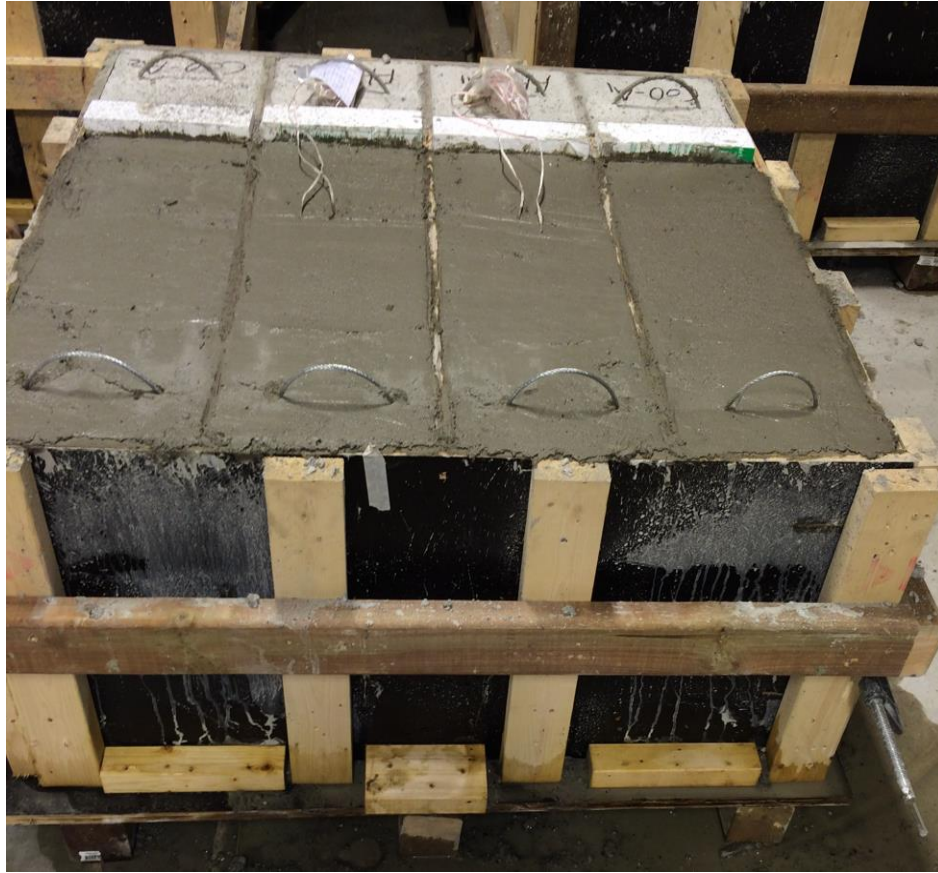


**Figure 3.9** Cast of top concrete

After the concrete hardened (one week later), the formworks (all the sidings) were removed for better curing of the concrete. The specimens were moist cured using wet burlap sheets wrapped around the specimens under a plastic sheet covering all the specimens [see Figures 3.10(a) and 3.10(b)]. Cylinders cast with the specimens were also moist cured under the same conditions of their corresponding specimens. The curing process extended for twenty-eight days. After that, each specimen was left and positioned in its vertical position and painted white to allows for easier surveillance of cracking during testing (see Figure 3.11).





(a) Wet burlap used for curing



(b) A plastic sheet covering all the specimens for curing

**Figure 3.10** Specimens moist curing





**Figure 3.11** Final shape of the test push-off specimen

### **3.4 Materials Properties**

#### **3.4.1 Steel Reinforcement**

As indicated previously in the description of the test specimens, 10M steel stirrups and bars in form of cages were used to strengthen the specimen against local bending and shear failures all around the specimen, as was shown in Figure 3.4. The control specimens (SS2-A1 and SS2-A2) were built with two 10M shear transfer steel stirrups of the same grade across its concrete interface (see Table 3.1).

The steel was supplied by a certified local dealer. It was a grade 400 steel having a young modulus of 200 GPa and yield strength of 400 MPa, as per the supplier information.

The steel used in this program conforms with the Canadian standard of carbon steel bars for concrete reinforcement, CSA G30.18 (2009).

### 3.4.2 GFRP Reinforcement

GFRP stirrups and GFRP headed bars were used across the shear planes of the push-off specimens. They were provided by V-Rod Canada, which is a Canadian FRP materials supplier. Both of stirrups and head bars had a nominal cross-sectional area of 126.7 mm<sup>2</sup>. However, stirrups were made of GFRP with a modulus of elasticity of 50 GPa, whereas, headed bars were of a higher GFRP grade with a modulus of elasticity of 60 GPa.

The used GFRP was sand coated to enhance the bonding properties of the material with the surrounding concrete and was made of longitudinal continuous fibers. The mechanical and other properties of the GFRP materials were provided by the supplier. Table 3.2 summarizes the most relevant physical and mechanical properties of these materials related to this research.

**Table 3.2** Properties of GFRP reinforcement

<b>Reinforcement</b>	<b>Cross section (mm<sup>2</sup>)</b>	<b>Ultimate tensile strength, <math>f_{Fu}</math> (MPa)</b>	<b>Tensile modulus <math>E_f</math> (GPa)</b>	<b>Ultimate tensile strain, <math>\epsilon_{fu}</math> (%)</b>
GFRP - Stirrup	126.7	1140	50	2.17
GFRP - Headed bar	126.7	1312	60	2.00

### **3.4.3 Concrete**

The first and second halves of all test specimens, were cast using a ready-mix concrete. It was provided by a local concrete supplier. The slump of the mix at the day of casting was measured and obtained a of 120 mm for both the first and the second patch.

During casting, compressive cylinders of 102 x 203 mm were prepared as well. For each half of specimen, two cylinders were made. These cylinders along with their companion specimens were moist cured together under the same conditions as described in section 3.3. The general procedure outlined in the ASTM C39 (2015) standard method for compressive strength of cylindrical concrete specimens, ASTM C39 (2015), was used to determine the compressive strength of the concrete. The cylinders were tested in the same day that their corresponding specimens were tested. Four concrete cylinders were tested and averaged for each test specimen. The average compressive strength of the tested concrete cylinders was about 35 MPa for all test specimens.

## **3.5 Instrumentations**

Using a Data Acquisition system (DAQ), the applied shear load and the shear slip parallel to the interface shear plane in addition to the strain of the internal shear transfer reinforcement were collected.

### **3.5.1 Shear Slip**

Special focus was directed to measure and carefully monitor the slip at different loading stages of the specimens. Two linear variable differential transducer (LVDT) were placed, one on each side of the specimen, parallel to the shear plane to measure the relative

slip between the two blocks of each specimen. The used LVDT is shown in Figure 3.12. The base of the LVDT was glued to the surface of the first block and the other end of it was rested against a metal bracket glued to the second block of the specimen. Upon loading, the first block starts to move relative to the other one causing the spring of the LVDT to compress which is read by the DAQ as the value of relative slip between the two concrete blocks. Since two LVDTs were used, the average value of both readings was considered later in the analysis, whenever applicable. Figure 3.13 shows the LVDT mounted on the surface of the specimen prior to the application of the shear load.



**Figure 3.12** The used linear variable differential transducer (LVDT)



**Figure 3.13** The LVDT mounted to the surface of the specimen

### **3.5.2 Reinforcement Strain Monitoring**

The strain in the internal shear transfer reinforcement crossing the shear plane of the test specimens was measured using electronic strain gauges attached to the surface of this reinforcement at the shear plane level, as shown in Figure 3.14. The strain is an important measure to assess the internal stress in the GFRP reinforcement utilizing its elastic property.

The first step of preparation for installation was to scrap off the sand coating over a small area just enough to fit the strain gauge. Extra caution was paid during the sand coating removal so that no extra FRP material was taken out so that the cross-sectional area of the

GFRP bar was preserved. The scraped area was carefully chosen to correspond to the interface level of the shear plane once the reinforcement is installed in the specimen. Afterwards, this area was cleaned using ethanol. It was then left to dry out before it was cleaned again using an acidic cleaner. Subsequently, the surface was treated using a water based alkaline surface cleaner. After the surface dried out, the strain gauge was glued to it using super glue. To prevent any damage to the strain gauges during the casting and vibration process, a thick coat of epoxy was laid on top of the strain gauge, after it was firmly secured to the bar surface.

Two strain gauges were used per specimen, except for the non-reinforced ones (C0-A1 and C0-A2), where there was no need for monitoring strain. The strain gauges were connected to the DAQ system where their readings were recorded and saved. The average value of both reading of the strain gauges were used as an average strain of the shear transfer reinforcement when the test results were analyzed.



**Figure 3.14** Electronic strain gauge glued to the surface of GFRP bar

### 3.6 Setup and Testing

The specimens were ready to test after about twenty-eight days of curing at which the desired strength of approximately 35 MPa was achieved. After painting each specimen with white paint, it was placed horizontally in its testing position. The specimen was placed on top of steel roller supports to eliminate the friction with the ground and allow for a free movement during the loading. On one end of the specimen, a hydraulic jack was used to apply the load and on the other side was in contact against a very stiff structural wall in the structural lab of the University of Windsor. The specimen was placed carefully so that the applied load would be concentric along the interface shear plane of the push-off specimen. A rubber sheet and a thick steel plate were placed between the specimen and the jack on one side and the specimen and the wall on the other side. The details of the test setup and instrumentations are shown schematically in Figure 3.15.

The loading process continued after the ultimate load was attained and the load started to drop. This loading condition allowed for better understanding of the post ultimate behavior of the concrete joints. The load was applied slowly at a rate of 10 kN per minute. The horizontal setup of the test specimens was chosen for its ease to setup and placing the specimen concentrically to the shear plane.



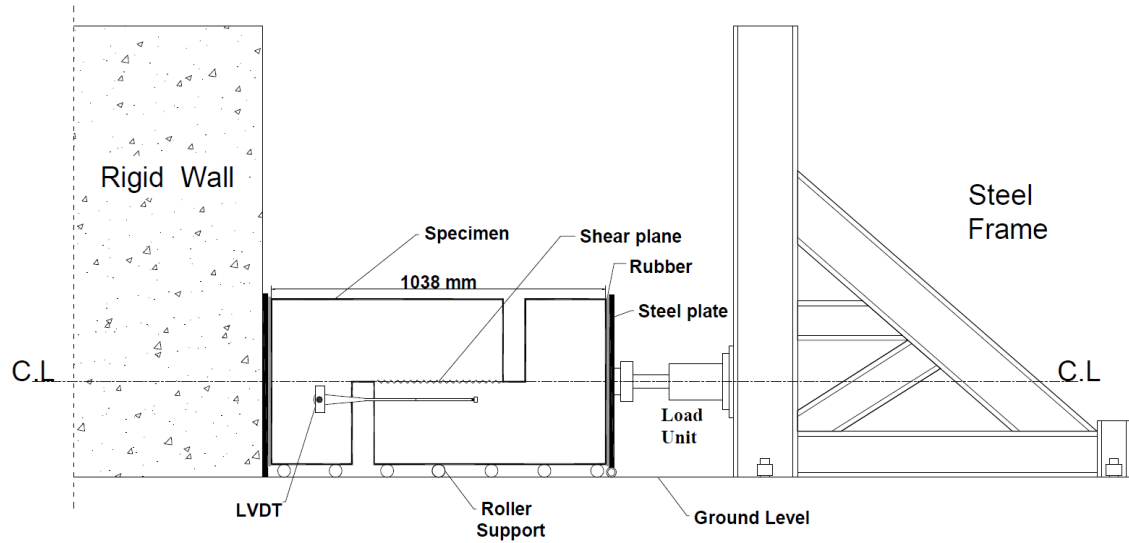


**Figure 3.15** Schematic drawing of the test setup

At every loading stage, the slip readings from both LVDTs and strain gauges were recorded by the DAQ. A photograph of a test specimen equipped with the LVDTs and connected to the DAQ, under the application of the load is shown in Figure 3.16.



**Figure 3.16** Test set-up



### **3.7 Summary**

The details of the push-off test specimens, their fabrication, and properties were described in this chapter. The materials used in fabricating these specimens were also listed along with their mechanical properties. All the steel reinforcement used in this study were of 10M bars and stirrups and they were locally supplied. According to the supplier's data, the steel reinforcement was of Grade 400 according to the Canadian standard CSA G30.18 (CSA, 2009). The Glass Fiber Reinforced Polymers (GFRPs) stirrups and headed bars, utilized in this investigation, were provide by V-Rod Canada. They were made of longitudinal fibers and they were sand coated. The process in which the specimens were fabricated was explained in detail. The instrumentations used to measure and collect the required data of the interfaces relative slip and reinforcement strain were defined along with their installation process. Testing procedure and setup were also explained in this chapter. In total twenty push-off specimens were prepared and tested to cover GFRP reinforcement ratio between 0.38% to 1.35% corresponding to stiffness in the range of 228 MPa and 811 MPa. The following chapter presents the results and their analysis.

## CHAPTER 4

### EXPERIMENTAL RESULTS AND DISCUSSION

#### 4.1 Introduction

The experimental results of the tested push-off specimens are presented and discussed. The test data are presented in terms of the relationships between the measured ultimate shear transfer stress and the longitudinal slip at the shear plane and the strain of the shear transfer reinforcement crossing that plane is illustrated. The shear transfer behavior of the tested specimens, the ultimate strength reported in terms of stresses, as the area of the shear plane of specimens of series A1 ( $100000 \text{ mm}^2$ ) was different from that of series A2 ( $75000 \text{ mm}^2$ ). In order to identify the influence of reinforcement stiffness on the shear transfer strength and behavior, the results of the specimens reinforced with GFRP headed bars from each series (A1 and A2) are presented together. Similar procedure is also followed for specimens with GFRP stirrups. The results of the control specimens containing steel shear transfer stirrups and no reinforcement are incorporated whenever necessary for comparison. This study is the second phase of an ongoing research to investigate the use of GFRP as shear transfer reinforcement. In the first phase (Alkatan, 2016), it was found that in order for the GFRP reinforcement to engage in the shear resisting mechanism, it has to be provided with a minimum reinforcement stiffness parameter ( $E\rho_v$ ) of 203 MPa. The GFRP reinforcement stiffness ( $E\rho_v$ ) used by Alkatan (2016) was in the range of 0 to 304 MPa. In the present study, the performance of GFRP shear transfer reinforcement is extended to higher reinforcement content corresponding to a stiffness as high as of 811 MPa.

## 4.2 Analysis of Test Results

The gathered test results of all the specimens are summarized in Table 4.1. In this table, the recorded ultimate shear transfer force and stress are reported as well as the corresponding values of the slip along the shear plane and the strain of the shear transfer reinforcement. The stiffness of the reinforcement used in each specimen is also listed for reference.

**Table 4.1** Test results

Specimen	$E\rho_v$ (MPa)	At Ultimate			
		$V_u$ (kN)	$v_u$ (MPa)	Slip (mm)	Reinforcement Strain ( $10^{-6}$ )
C0-A1	0	342.94	3.43	0.41	-
SS2-A1	800	281.28	2.81	0.39	2486.17
FS2-A1	253	267.84	2.68	0.34	2208.58
FS3-A1	380	489.44	4.89	0.72	5961.96
FS4-A1	507	428.61	4.29	0.11	3976.04
FH3-A1	228	328.00	3.28	1.00	5993.25
FH4-A1	304	293.54	2.94	0.37	2382.61
FH5-A1	380	497.08	4.97	0.67	6987.77
FH6-A1	456	547.09	5.47	0.80	5752.28
FH8-A1	608	549.75	5.50	1.00	5889.40
C0-A2	0	216.50	2.89	0.28	-
SS2-A2	1067	189.04	2.52	0.83	2342.85
FS2-A2	338	172.09	2.29	0.41	3112.89
FS3-A2	507	274.64	3.66	0.92	8828.44
FS4-A2	676	484.14	6.46	0.94	3618.79
FH3-A2	304	212.97	2.84	0.97	6563.44
FH4-A2	405	217.80	2.90	0.30	2308.43
FH5-A2	507	264.21	3.52	1.00	9009.55
FH6-A2	608	303.91	4.05	0.60	3542.50
FH8-A2	811	397.24	5.30	0.97	6081.31

#### 4.2.1 Load-Slip Behavior

The load-slip curves of specimens with GFRP stirrups of series A1 (FS2-A1, FS3-A1 and FS4-A1) are shown in Figure 4.1 along with the curves of the control specimens of the same series SS2-A1 and C0-A1. The failure of the unreinforced specimen C0-A1 was brittle and sudden with no sign of damage. The load kept increasing up to the ultimate point at which the shear plane suddenly cracked and the specimen split into its two concrete blocks. The load has dropped to zero at this point. The corresponding slip at the ultimate point was a small value of 0.41 mm (slip in SS2-A1 was even smaller).

However, when shear transfer reinforcement was utilized with GFRP stirrups or steel stirrups, the applied shear increased with the slip up to the ultimate with a gradual development of the cracking of the shear plane. In this case, the load dropped but the slip increased, however, shortly after, the reinforced specimens maintained its resistance. From Figure 4.1, it can be seen that the drop of the load after the ultimate point was smaller when GFRP stirrups were used compared to that of the steel reinforced specimen. Furthermore, the resistance post peak was more significant for specimens with GFRP stirrups. In this case, 90 to 100% of the ultimate load was maintained up to a high value of slip.

In a similar fashion, the shear stress-slip behaviors of specimens of series A2 with GFRP stirrups and control specimens SS2-A2 and C0-A2 are shown in Figure 4.2. Similar observations and notes reported for series A1 are applicable here too. However, the steel reinforced specimen of series A2 showed a better post ultimate resistance as compared to the same specimen of series A1. Specimens with GFRP stirrups of both series A1 and A2 had limited values of slip at the ultimate load, which were less than 1.00 mm (see Table

4.1). The slips of control specimens C0-A1, C0-A2, SS2-A1 and SS2-A2 at the ultimate were 0.41, 0.28, 0.39 and 0.83 mm, respectively.

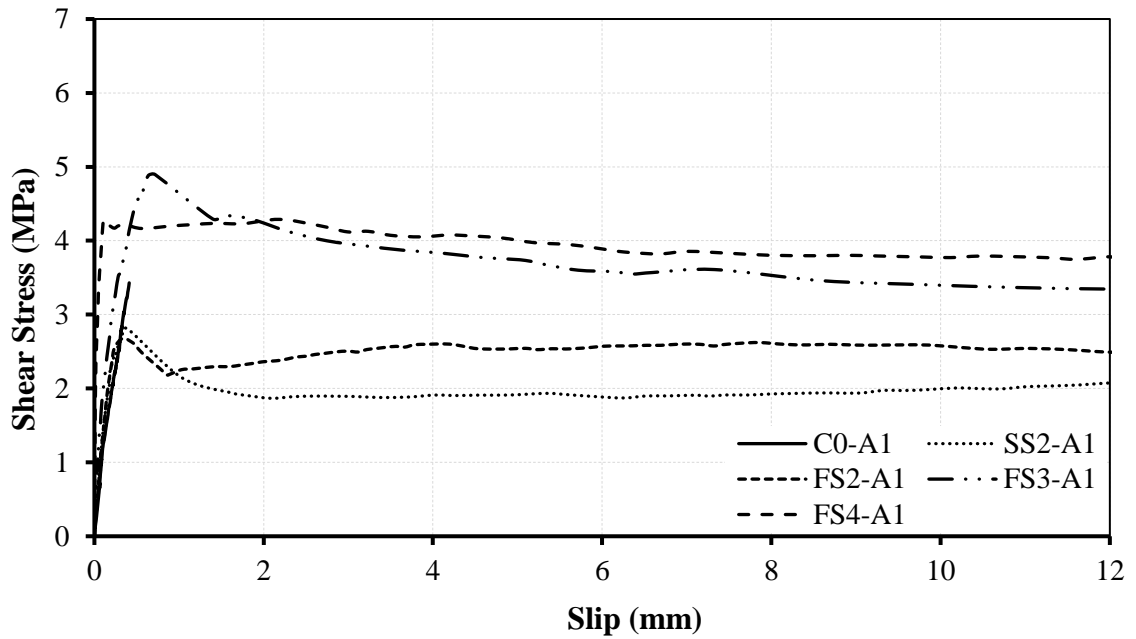


**Figure 4.1** Load-Slip behavior of specimens of series A1 with stirrups shear transfer reinforcement and unreinforced specimen

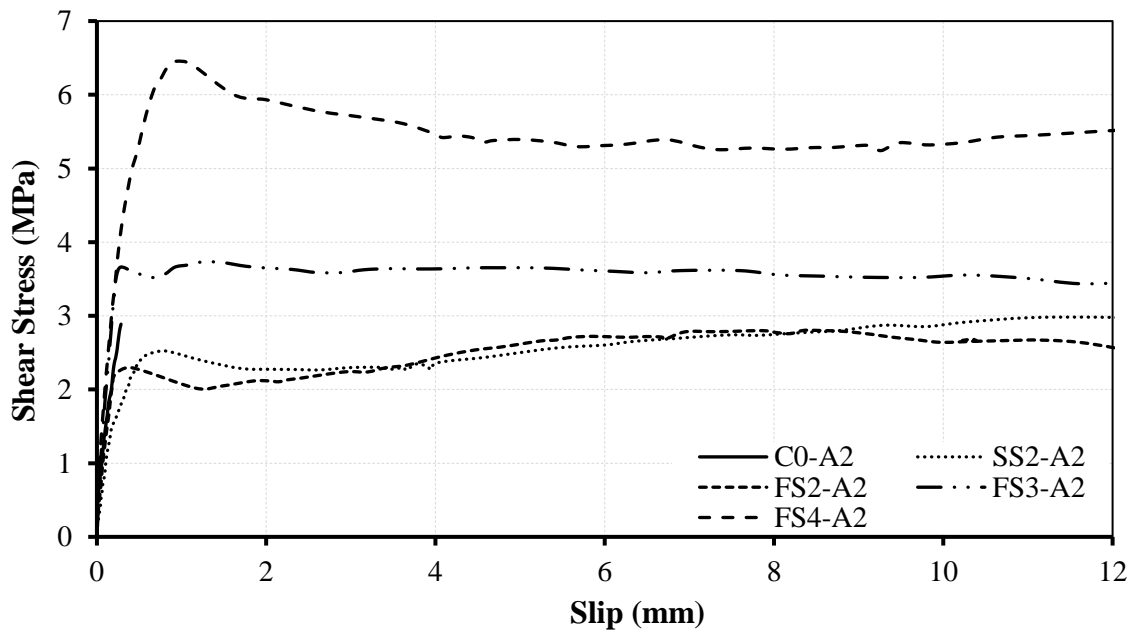


**Figure 4.2** Load-Slip behavior of specimens of series A2 with stirrups shear transfer reinforcement and unreinforced specimen

The shear stress-slip response of specimens with GFRP headed bars of series A1 and A2 are illustrated in Figures 4.3 and 4.4. In these figures, the behaviors of the control specimens C0-A1 and C0-A2 are also included for comparison.

The ultimate strength of all the headed GFRP bars reinforced specimens was attained at a slip value in the range of 0.30 to 1.00 mm. Similar observation of post ultimate strength reported earlier for specimens with GFRP stirrups can also be noted here for the case when GFRP headed bars were used in A1 and A2 series, as shown in Figures 4.3 and 4.4. However, the post ultimate capacity associated with GFRP headed bars was much higher. The maximum shear transfer resistance post to ultimate reached 160% of the ultimate load for specimen FH4-A2, whereas, it reached a maximum value of 164% of the ultimate load for FH3-A2. The superiority post ultimate resistance associated with GFRP headed bars shear transfer reinforcement was also reported by Alkatan (2016), which was related to the superior bond and dowel action characteristics of the headed bars.

The post ultimate strength resistance was observed at a slip values between 1 to 2 mm after the slight drop of the load beyond the ultimate point (see Figures 4.1 to 4.4). This resistance continued, at different levels, up to high values of relative slip (higher than 7 mm).

The post ultimate resistance observed for the GFRP reinforced test specimens was attributed to the dowel action of the reinforcing bars crossing the interface (Alkatan, 2016; Paulay et al. 1974).

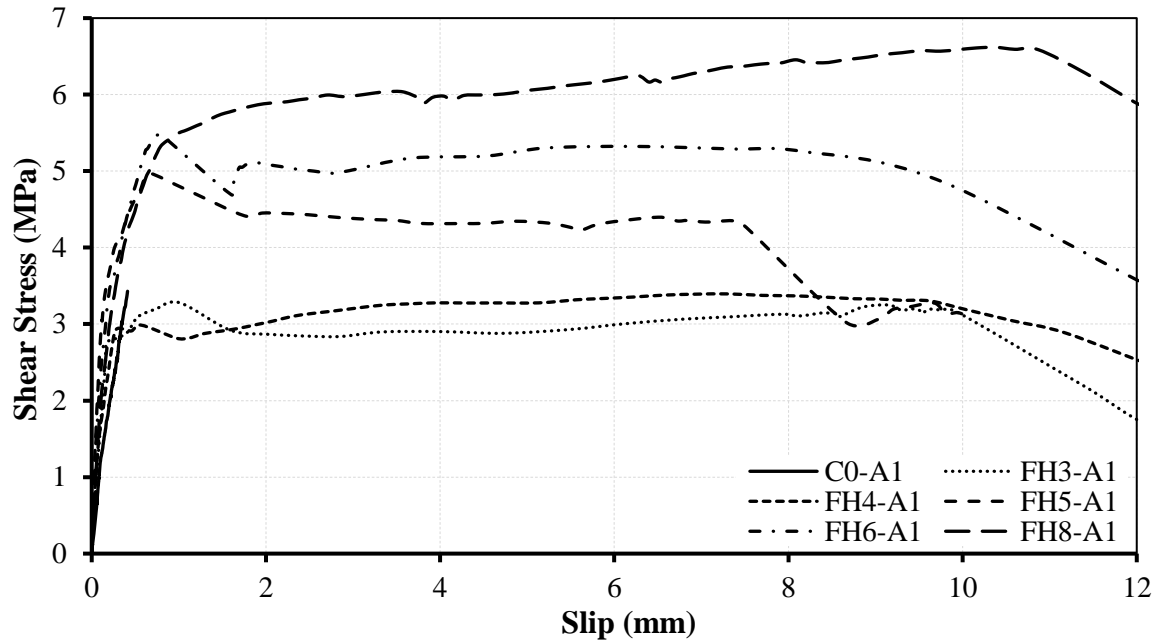


**Figure 4.3** Load-Slip behavior of specimens of series A1 with headed bars shear transfer reinforcement and unreinforced specimen

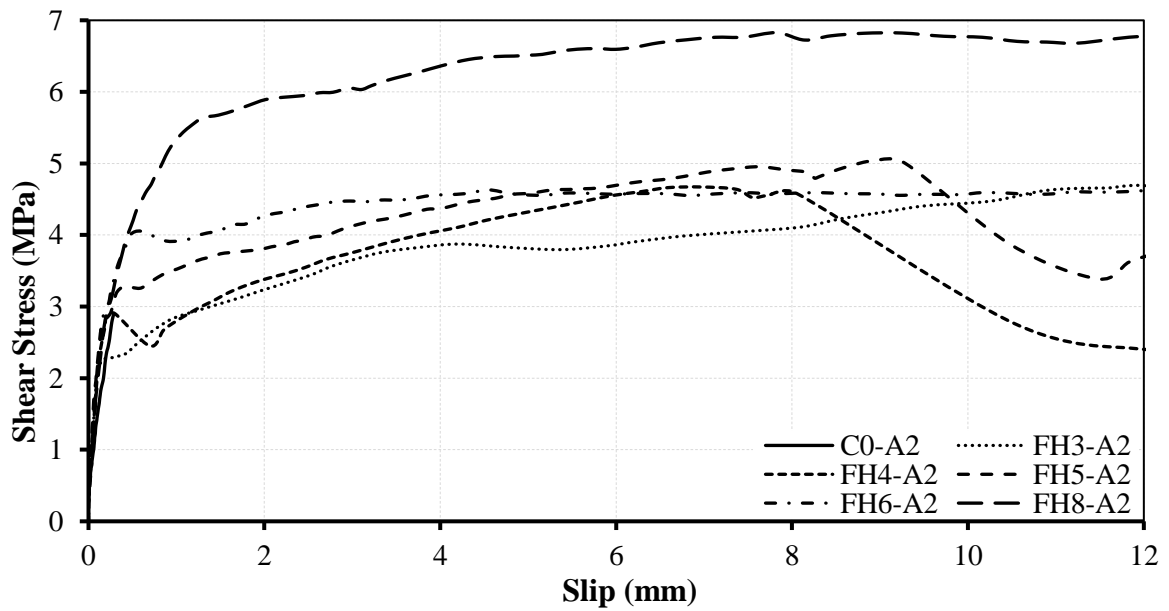


**Figure 4.4** Load-Slip behavior of specimens of series A2 with headed bars shear transfer reinforcement and unreinforced specimen

In the light of the shown results, the general load-slip behavior of GFRP reinforced specimens conforms with the three-phases behavior proposed by Alkatan (2016) as shown in Figure 4.5. Prior to cracking, the load is taken mainly by the concrete interface with no effective contribution from the shear transfer reinforcement. The fully cracked shear plane is developed over two stages. The first stage involves the resistance provided by the mechanical bonding between the concrete surfaces of the interfaces. After the bond is destroyed, the load is then carried by the interlocking between the asperities on both concrete surfaces of the interface shear plane up to the cracking point. At the cracking point, the slip values are very limited as well as the strain in the reinforcement crossing the shear plane.

After the shear plane is fully cracked, the stiffness of the specimen decreases as illustrated in Figure 4.5. In this phase (post-cracked phase), the load is resisted by the friction provided by the roughness of the concrete interface and the clamping stresses delivered by the shear transfer reinforcement. Upon cracking, the two blocks of the specimen slide along the shear plane relative to each other. Due to the irregularity of the interface surface the sliding movement will be associated with a widening of the shear plane, which would place the reinforcement across this in tension. This would cause balancing compressive stresses along the shear plane causing a frictional shear resistance.

The slip values at the ultimate loads of the tested specimens were found not to exceed 1.00 mm at all times, which is in agreement with the previous findings of Alkatan (2016) for GFRP shear transfer reinforcement and others such as, Harries et al. (2012), Loov and Patnaik (1994) and Mattock (1974) for steel shear transfer reinforcement.



Post to the ultimate point, the load drops with an increase of the slip up to a slip in the range of 1 to 2 mm, where the dowel action of the GFRP reinforcing bars is engaged in the shear resistance. Similar observations were noted by Alkatan (2016) when GFRP reinforcement was used. It is worth mentioning that the post ultimate resistance associated with steel reinforcement was found to take place at a slip between 2.5 to 3 mm (Paulay et al. 1974).

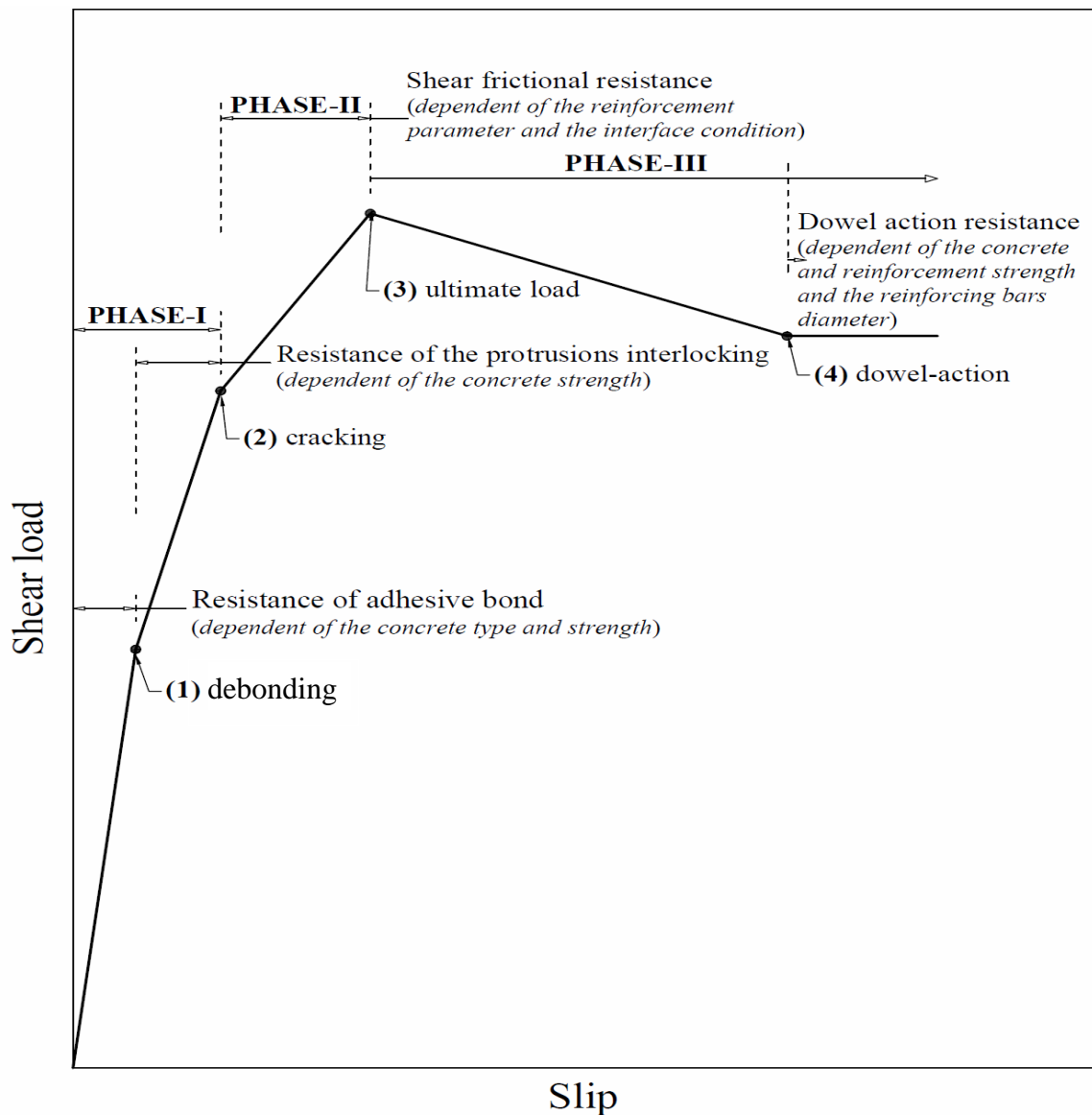


**Figure 4.5** General load-slip behavior (Alkatan 2016)

#### 4.2.2 Load-Reinforcement Strain Behavior

The relationships between the applied shear stress and the strain along the steel stirrups of the specimens SS2-A1 and SS2-A2 are shown in Figure 4.6. It can be noted from the load-strain curve of SS2-A1 that the strain in the steel stirrups was very small (229 microstrain) at the end of phase 1 (stress of 1.64 MPa). The strain started to increase at a higher rate with the load and reached a value of 2486 microstrain at the ultimate load which is close to the yielding strain.

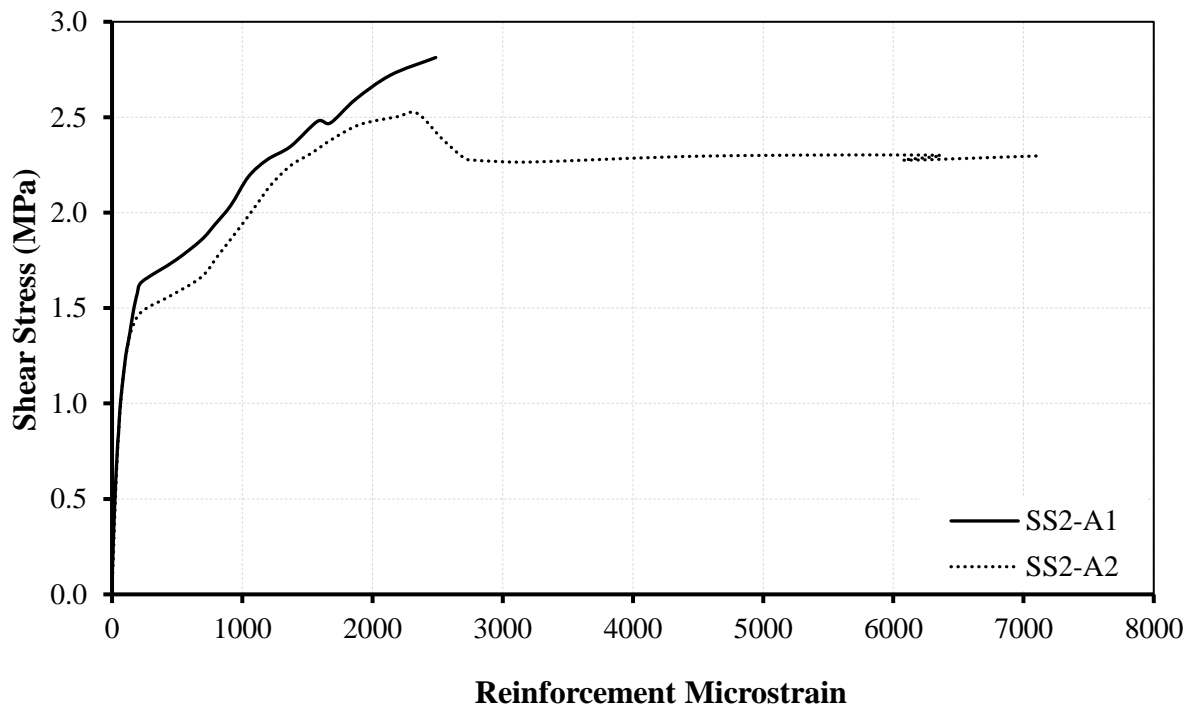


**Figure 4.6** Load-Strain behavior of specimens SS2-A1 and SS2-A2

Similar notes can be taken from the load-strain curve for specimen SS2-A2. Prior to cracking and at a shear stress of 1.48 MPa, the strain in the steel stirrups was about 227 microstrain. However, from this point forward, the strain increased at a higher rate and reached a value of 2342 microstrain at the ultimate load. These observations support the

findings of the previous studies in which the steel was found to yield at the ultimate shear transfer strength (Hofbeck et al. 1969; Mattock and Hawkins, 1972; Mattock 1974; Loov and Patnaik 1994; Alkatan 2016). After reaching the ultimate load and the steel yields, the capacity starts to drop with an increasing strain.

Figures 4.7 and 4.8 illustrate the relationship between the applied shear stress and the strain in the GFRP stirrups for specimens of the series A1 and A2, respectively. It is noted, from both figures, that the strain level in the GFRP stirrups remained small up for stress level within the range of 2 to 3 MPa. The minimum strain in the GFRP stirrups within this range was reported for specimen FS4-A2, which was about 166 microstrain and the maximum strain was for specimen FS4-A1 (621 microstrain). This is very also close to what was found by Alkatan (2016), where the cracking stress was suggested to be in the range of 2 to 2.7 MPa. Within this range, the strain in the GFRP reinforcement is very small indicating the marginal role of the GFRP reinforcement in resisting the shear prior to cracking.

Subsequently, the strain in the GFRP stirrups started to increase rapidly with the load. However, the rate at which the load increased was lower in this stage than it was in the stage prior to cracking. This indicates the engagement of the GFRP shear transfer reinforcement in the shear transfer resisting mechanism.

At ultimate load, the strain of the GFRP stirrups of specimens of series A1 and A2 was higher than 3000 microstrain with an average value of 4600 microstrain. It can also be noted from Figures 4.7 and 4.8 that after the ultimate was attained, a significant resistance was maintained at larger slip and high levels of strain. The specimen's strength, when the

GFRP stirrups were used, did not drop dramatically after the ultimate as in the case when steel stirrups were utilized (see Figure 4.6).

For interfaces intersected by GFRP reinforcement having a stiffness parameter ( $E\rho_v$ ) equals to or higher than 203 MPa, the ultimate loads were found to correspond to a strain level in the range of 3000 to 5000 microstrain and a design optimum value of 5000 microstrain was recommended for the design (Alkatan 2016). Since all the GFRP reinforced specimens used in this study had a stiffness parameter higher than 203 MPa, the findings reported herein are consistent with the previous research.

The load-strain behaviors of specimens with GFRP headed bars from series A1 and A2 are reported in Figures 4.9 and 4.10, respectively. Similar to what was described above for GFRP stirrups, the strain in the headed bars was very limited prior to cracking within the shear stress of 2 to 3 MPa. The strain began to increase under the application of the shear load. In most of the headed bars in the test specimens the strain reached a value higher than 3000 microstrain. However, when headed bars were used, the load after the ultimate capacity was maintained or slightly increased with the increase of strain giving a notable post peak resistance that is more effective than it was for the GFRP stirrups. The maximum post ultimate resistance in the GFRP reinforced specimens were considerably high, from 96% for FH5-A1 up to 164% of the ultimate for FH3-A2. This behavior was attributed to the better bond and dowel action characteristics associated with GFRP headed bars (Alkatan 2016).

In this study, the stiffness parameter ( $E\rho_v$ ) of the headed bars in the test specimens were all higher than 203 MPa ranging from 228 to 811 MPa. Similar to the GFRP stirrups,

a 5000 microstrain can be considered as a reasonable estimate for the strain in the GFRP headed bars at the ultimate load.

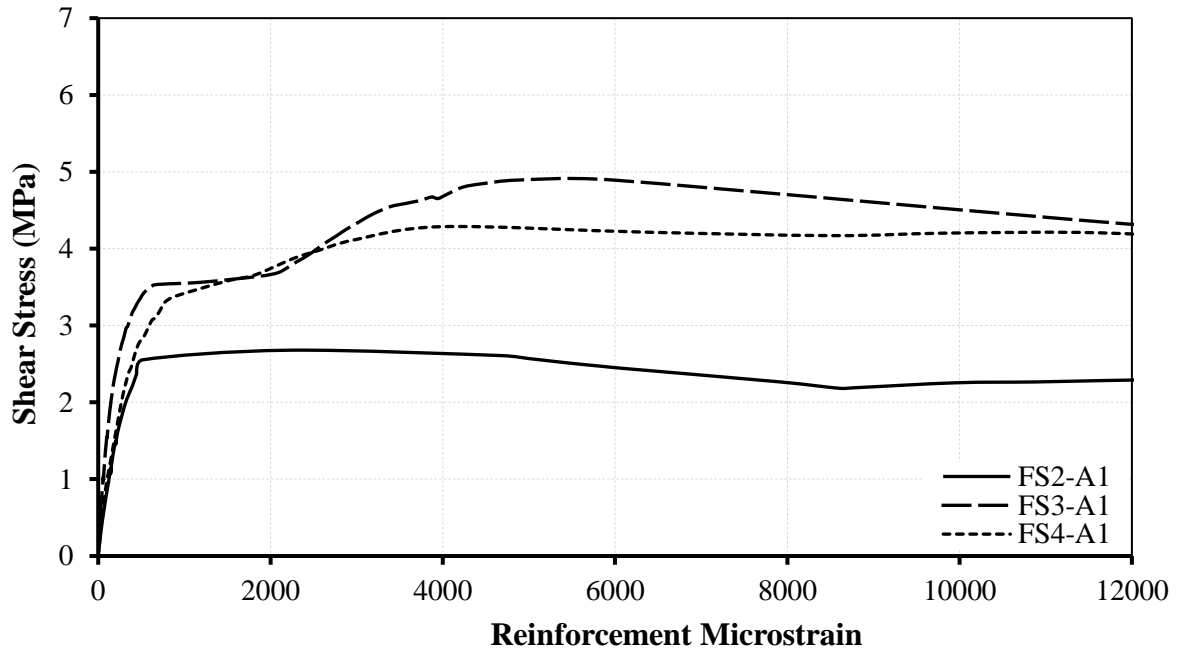


**Figure 4.7** Load-Reinforcement Strain behavior of specimens with GFRP stirrups of series A1

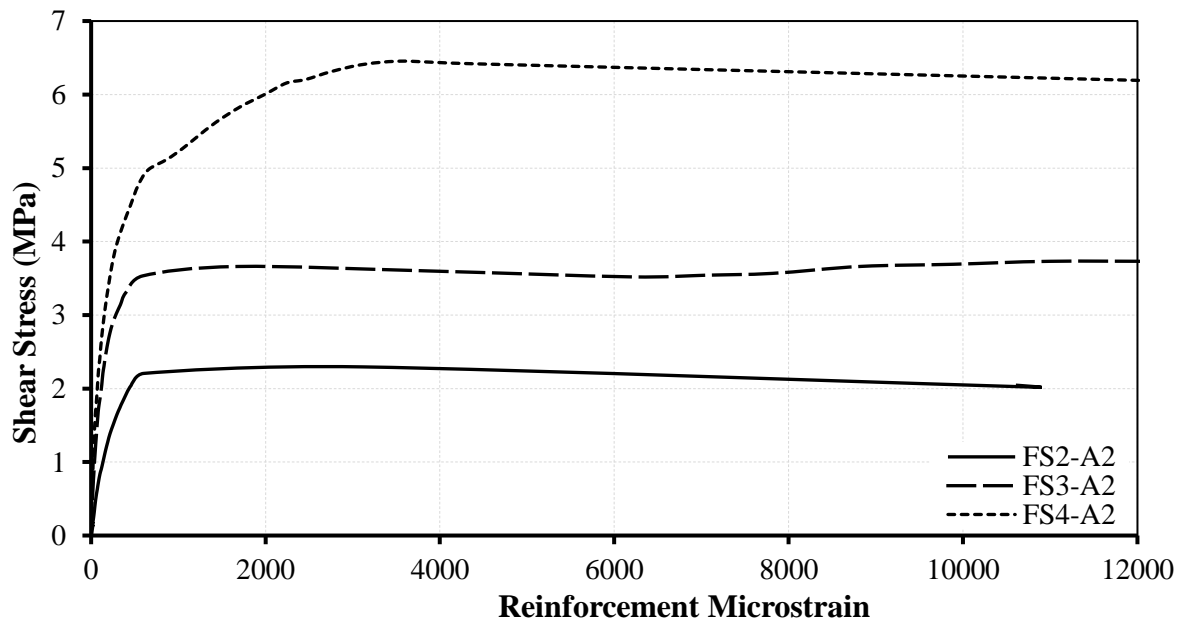


**Figure 4.8** Load-Reinforcement Strain behavior of specimens with GFRP stirrups of series A2

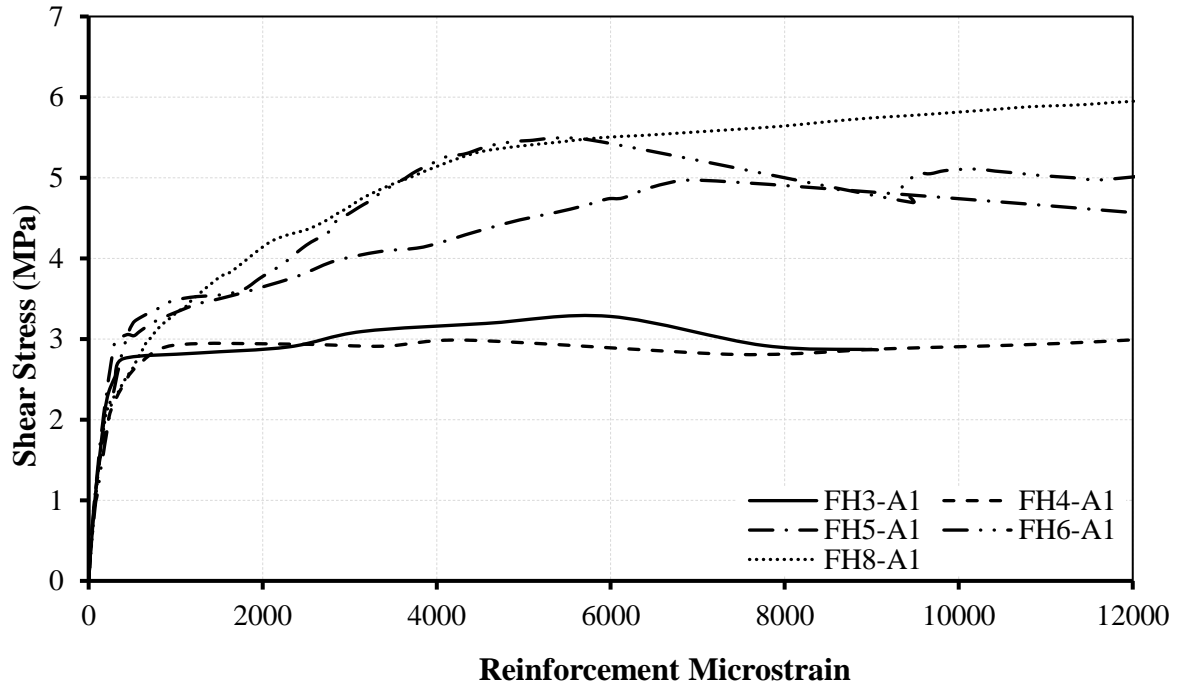


**Figure 4.9** Load-Reinforcement Strain behavior of specimens with GFRP headed bars of series A1

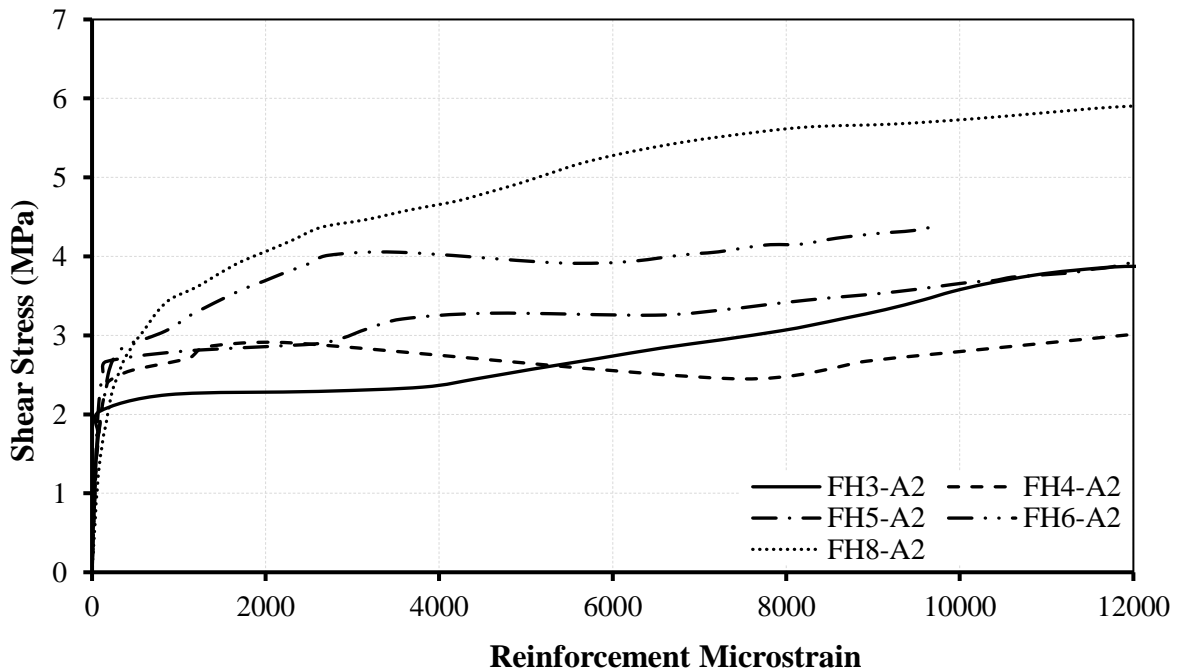


**Figure 4.10** Load-Reinforcement Strain behavior of specimens with GFRP headed bars of series A2

#### 4.2.3 Effect of Reinforcement Stiffness Parameter ( $E\rho_v$ )

In the proceeding section, the test specimens with similar reinforcement stiffness and shape were compared to study the influence of the reinforcement stiffness on the shear capacity. In the present section, we are interested to compare specimens with the same stiffness and reinforcement shape but with different contact surface. Three groups of specimens, I, II and III are listed in Table 4.2. The reinforcement stiffness parameter ( $E\rho_v$ ), strength ( $v_u$ ), slip and reinforcement strain for the two specimens of each group are also reported in Table 4.2. Group I consists of specimens FS4-A1 and FS3-A2, which both have a stiffness parameter of 507 MPa. The shear transfer strengths of these specimens were 4.29 and 3.66 MPa, respectively. Similarly, specimens FH4-A1 and FH3-A2 of group II, both having a stiffness parameter of 304 MPa, had relatively close shear strengths of 2.94 and 2.84 MPa, respectively. The specimens of the third group with 608 MPa reinforcement stiffness parameter, FH8-A1 and FH6-A2, had ultimate strengths of 5.50 and 4.05 MPa, respectively. The results reported in this work are consistent with previous findings of Alkatan (2016) that the shear transfer strength is mainly correlated to the reinforcement stiffness. Specimens with similar reinforcement stiffness parameter and shape were found to result in similar shear transfer capacities.

**Table 4.2** Groups of specimens having similar reinforcement shape and stiffness parameter

Group	Specimen	$E\rho_v$ (MPa)	At Ultimate			
			$V_u$ (kN)	$v_u$ (MPa)	Slip (mm)	Reinforcement Strain ( $10^{-6}$ )
I	FS4-A1	507	428.61	4.29	0.11	3976.04
	FS3-A2	507	274.64	3.66	0.92	8828.44
II	FH4-A1	304	293.54	2.94	0.37	2382.61
	FH3-A2	304	212.97	2.84	0.97	6563.44
III	FH8-A1	608	549.75	5.50	1.00	5889.40
	FH6-A2	608	303.91	4.05	0.60	3542.50

Table 4.3 compares the experiment results of specimens with the same stiffness but with different reinforcement shape. Two groups of test specimens (groups I and II) are reported. Specimens of group I of three GFRP stirrups FS3-A1 and five headed bars FH5-A1 both have a stiffness parameter of 380 MPa. The measured shear transfer strengths of these specimens were 4.89 and 4.97 MPa, respectively. Likewise, group II specimens FS4-A1, FS3-A2 and FH5-A2, all have stiffness of 507 MPa. The shear capacity at the ultimate state are comparable. The measured ultimate shear transfer strengths for group II were 4.29, 3.66 and 3.52 MPa, respectively. These observations conform with the previous conclusion that was drawn in section 4.2.1 where the influence of the reinforcement shape was mainly observed at the post ultimate stage. The shape of the GFRP reinforcement was found to have no significant effect on the shear transfer strengths of the push-off specimens prior to the post ultimate stage.

**Table 4.3** Groups of specimens having different reinforcement shape and similar stiffness parameter

Group	Specimen	$E\rho_v$ (MPa)	At Ultimate			
			$V_u$ (kN)	$v_u$ (MPa)	Slip (mm)	Reinforcement Strain ( $10^{-6}$ )
I	FS3-A1	380	489.44	4.89	0.72	5961.96
	FH5-A1	380	497.08	4.97	0.67	6987.77
II	FS4-A1	507	428.61	4.29	0.11	3976.04
	FS3-A2	507	274.64	3.66	0.92	8828.44
	FH5-A2	507	264.21	3.52	1.00	9009.55



To further illustrate the influence of the reinforcement stiffness, all the test results of the push-off specimens are listed in Table 4.4 ascendingly according to the specimens' reinforcement stiffness parameters ( $E\rho_v$ ) and grouped by reinforcement type and shape. Table 4.4 includes three groups of specimens based on the shape of the used GFRP reinforcement. Specimens with GFRP stirrups are tilted as of group II and specimens with GFRP headed bars in group III. Also, the two unreinforced specimens of both series A1 and A2 are listed under group I ( $E\rho_v = 0$ ). It can be observed that increasing the stiffness parameter among each group specimens, resulted in an increase of the ultimate strength. For example, raising the stiffness from 253 MPa for FS2-A1 to 676 MPa for FS4-A2 (166% increase), led to an increase of about 141% in the shear transfer capacity. Similarly, specimen FH5-A1 with a reinforcement stiffness parameter of 380 MPa, that is 25% higher than that of specimen FH4-A1 (304 MPa), had an ultimate shear transfer strength 69% greater than the strength of FH4-A1. The relationship between the measured ultimate shear transfer strength ( $v_u$ ) and the reinforcement stiffness ( $E\rho_v$ ) is represented in Figure 4.19 (refer to section 4.2.5). These results that are drawn from this table accompanied with Figure 4.19 suggest that the shear transfer strength is directly related to the GFRP reinforcement stiffness. Clearly, increasing the reinforcement stiffness across a concrete joint increases its shear transfer resistance.

**Table 4.4** Test results arranged ascendingly according to the reinforcement stiffness parameter

Group	Specimen	$E\rho_v$ (MPa)	At Ultimate			
			$V_u$ (kN)	$v_u$ (MPa)	Slip (mm)	Reinforcement Strain ( $10^{-6}$ )
I	C0-A1	0	342.94	3.43	0.41	-
	C0-A2	0	216.50	2.89	0.28	-
II	FS2-A1	253	267.84	2.68	0.34	2208.58
	FS2-A2	338	172.09	2.29	0.41	3112.89
	FS3-A1	380	489.44	4.89	0.72	5961.96
	FS3-A2	507	274.64	3.66	0.92	8828.44
	FS4-A1	507	428.61	4.29	0.11	3976.04
	FS4-A2	676	484.14	6.46	0.94	3618.79
III	FH3-A1	228	328.00	3.28	1.00	5993.25
	FH3-A2	304	212.97	2.84	0.97	6563.44
	FH4-A1	304	293.54	2.94	0.37	2382.61
	FH5-A1	380	497.08	4.97	0.67	6987.77
	FH4-A2	405	217.80	2.90	0.30	2308.43
	FH6-A1	456	547.09	5.47	0.80	5752.28
	FH5-A2	507	264.21	3.52	1.00	9009.55
	FH8-A1	608	549.75	5.50	1.00	5889.40
	FH6-A2	608	303.91	4.05	0.60	3542.50
	FH8-A2	811	397.24	5.30	0.97	6081.31

#### 4.2.4 Failure Modes

As mentioned in the previous section, specimens with no reinforcement across their shear plane, C0-A1 and C0-A2, developed a very brittle and sudden failure mode. The failure occurred by a total splitting of the concrete interface which resulted in breaking of the specimens into their own two L-shaped concrete blocks. This mode of failure is shown in Figures 4.11 and 4.12.



**Figure 4.11** Failure mode of unreinforced specimen C0-A2



**Figure 4.12** Splitting of specimen C0-A1

When steel shear transfer stirrups were used across the shear plane of specimens SS2-A1 and SS2-A2, the failure was relatively less brittle compared to C0-A1 and C0-A2. However, after the ultimate load was reached the load dropped quickly with the increase of the slip. At higher values of slip, a considerable amount of concrete spalling around the stirrups was observed in both specimens SS2-A1 and SS2-A2, as shown in Figures 4.13 and 4.14.



**Figure 4.13** Concrete spalling in specimen SS2-A1



**Figure 4.14** Concrete spalling in specimen SS2-A2



The failure modes of specimens containing GFRP reinforcement across their shear plane was a ductile failure. As it was discussed in the previous section, GFRP reinforced specimens showed a sizable post ultimate resistance. However, similar to the case of specimens with steel stirrups specimens with GFRP stirrups suffered from concrete cover spalling but it was at a higher extent. Figures 4.15 and 4.16 shows the extensive amount of spalling occurred in specimens FS2-A1 and FS3-A1 respectively.



**Figure 4.15** Concrete spalling in specimen FS2-A1



**Figure 4.16** Concrete spalling in specimen FS3-A1

This type of failure mode was also noted by Alkatan (2016), where a broad spalling of the concrete cover occurred. It was suggested at the time that the widespread spalling associated with GFRP stirrups is caused by the higher stress levels in the GFRP bars at a progressive loading stages as compared to the steel rebars. This is consistent with the observations made in this study and the high strain levels measured in the GFRP bars during the post ultimate loading stage.

GFRP headed bars were the best option to deliver sizable ductile failure modes. For specimens with three headed bars from both series no concrete spalling was reported. However, for specimens with congested reinforcement across their shear plane such as those with four headed bars and higher, concrete spalling occurred. The spalling in this

case occurred at higher values of slip as compared to the case of stirrups. Figure 4.17 illustrates the failure mode of the specimens with six headed bars of series A2, FH6-A2.



**Figure 4.17** Failure mode of specimen FH6-A2

Having concrete spalling at higher slips in the GFRP headed bars specimens is believed to be attributed to the fact that the headed bars have thicker concrete cover than what could be provided for the 200 mm wide GFRP stirrups. The width of the stirrup allowed for about 25 mm cover from each side, which was shown to be sufficient up to the ultimate load and not adequate at an advanced loading stages (Alkatan 2016). Some of the GFRP headed bars in the specimens that showed significant resistance post to ultimate



capacity, were able to reach their ultimate strength and ruptured under the application of the shear load (Figure 4.18).

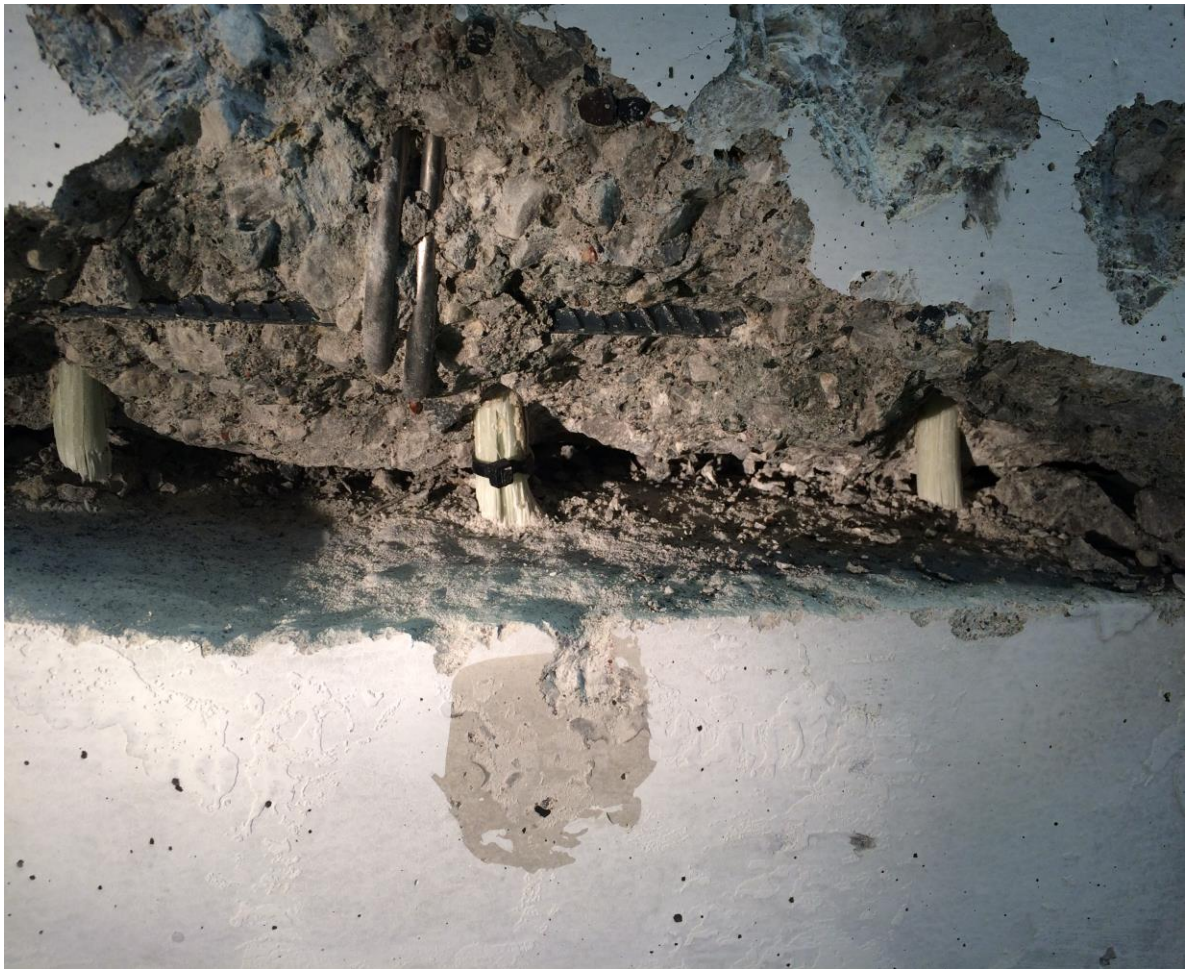


**Figure 4.18** Rupture of headed bars in specimen FH6-A1

#### 4.2.5 Ultimate Strength

It was mentioned in the literature review of this thesis that one of the main assumptions of the shear friction theory was that the steel across the concrete shear interface yields at the ultimate load. According to this theory the ultimate shear transfer strength is reached at the point where steel yields (Birkeland and Birkeland 1966; Mast, 1968). This assumption ignores any further contribution of the dowel action of the steel bars since it was associated with higher slips that occur post to the yielding of steel (Paulay et al. 1974; Khan and Mitchell, 2002).

Furthermore, the shear friction theory considers a cracked interface prior to the application of the shear load and disregards the contribution of the concrete surface to the shear transfer resistance. The modified shear friction hypothesis developed later-on, included the influence of the cohesion provided by the concrete surface (Mattock, 1974; Mattock and Hawkins, 1972). The cohesion stress provided by the concrete surface was further investigated and was correlated with concrete compressive strength ( $f'_c$ ) of the shear interface (Mattock, 1988; Khan and Mitchell 2002; Harries et al. 2012; Alkatan, 2016). However, the assumption of yielding of steel shear transfer reinforcement at the ultimate load remained valid in the modified shear friction theory and it is widely accepted.

As it was discussed in the literature review, other researchers, suggested different values of the coefficient of friction ( $\mu$ ) depending on their test results with various conditions of the shear interface. In addition, many expressions that include the influence of the concrete strength ( $f'_c$ ) on the cohesion stress of the concrete surface were also recommended.

Since the GFRP material is assumed to remain elastic up to its rupture point with no yielding point, a different ultimate limit state was proposed. According to Alkatan (2016) who first investigated the performance of Fibre Reinforced Polymer (FRP) material across the concrete-concrete interfaces, a strain limit of 5000 microstrain in the GFRP reinforcement was recommend at the ultimate shear transfer strength. This could also be confirmed based on the results obtained in this study which was discussed in details in section 4.2.2 of this chapter. Furthermore, cold joint interfaces with natural roughness formed by casting concrete on both sides of the shear plane at different times, was used by Alkatan (2016). For this type of surface, a value of 1 for the coefficient of friction was proposed for as-cast rough concrete-concrete interfaces which was consistent with the recommendation of previous studies for rough interfaces.

In the later mentioned study, the shear friction theory was adopted to describe the shear transfer along concrete joints intersected by GFRP reinforcement and the following general form expression for the shear transfer strength was proposed:

$$v_u = c + \mu \varepsilon_F E_F \rho_v \sin \alpha_f + \varepsilon_F E_F \rho_v \cos \alpha_f \quad (4.1)$$

where  $c$  is the cohesion stress delivered by the concrete interface,  $\mu$  is the confection of friction ( $\mu = 1$ ),  $\varepsilon_F$  is the strain in the GFRP reinforcement at the ultimate ( $\varepsilon_F = 5000$  microstrain),  $E_F$  is the modulus of elasticity of the used GFRP reinforcement,  $\rho_v$  is the reinforcement ratio and  $\alpha_f$  is the angle of inclination of the reinforcement relative to the shear plane. The cohesion stress,  $c = 0.05f'_c$ , was recommended for the average strength of the test results, however, for design purposes the author recommended that the cohesion should be taken as  $0.04f'_c$  which corresponds to the lower bound of the results.

For reinforcement placed perpendicular to the shear plane, which is the case in the specimens of the current study ( $\alpha_f = 90^\circ$ ) and a lower bound condition ( $c = 0.04f'_c$ ), Eq. 4.1 can be rewritten as follows:

$$v_u = 0.04f'_c + 0.005E_F\rho_v \quad (4.2)$$

In Figure 4.19, the shear transfer strength ( $v_u$ ) is plotted as function of the reinforcement stiffness parameter ( $E_F\rho_v$ ). The two parameters are normalized relative to the concrete strength (divided by  $f'_c$ ). The figure incorporates the test results of Alkatan (2016) with the ones of the current study.

Eq. 4.2 is presented by the solid line in Figure 4.19. Since most of the test points are above the equation's line, it appears to give a rational and conservative prediction of the shear transfer strength of as-cast concrete joints when GFRP is used as a shear transfer reinforcement.

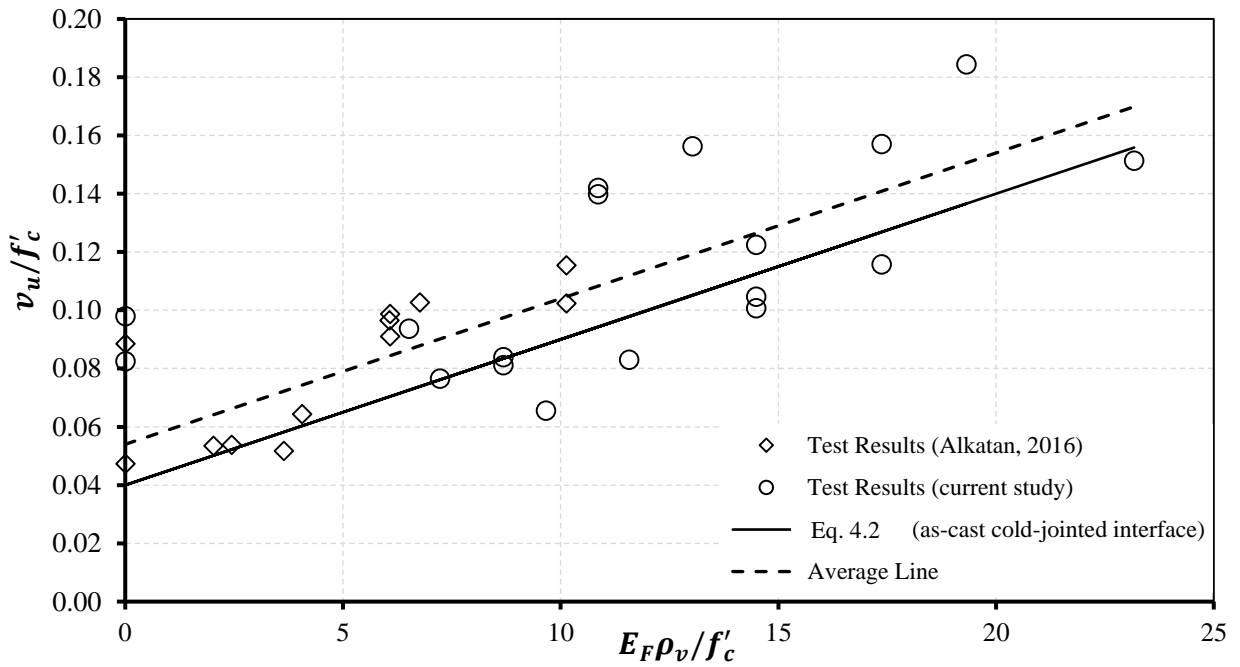


**Figure 4.19** Test results and Eq. 4.2

The average shear strengths of the test specimens are also represented by the dashed line on this figure. As it can be seen, this line has the same slope of the recommended prediction expression line (Eq. 4.2), but with higher amplitudes. Hence, for a conservative evaluation of the shear transfer strength of concrete-to-concrete interfaces, Eq. 4.2 is thought to be more appropriate.

### **4.3 Summary**

In the present chapter, the results of the test specimens were discussed. The load-slip behaviors of specimens of series A1 and A2 having no reinforcement, steel stirrups, GFRP stirrups and GFRP headed bars across their shear plane were presented. The general relationship between the applied shear load and slip that was proposed by Alkatan (2016) was verified to be equally applicable for the specimens of the present research. Furthermore, the variation of the applied load was plotted against the strain measured along the shear transfer reinforcement and commented on. The different failure modes of the specimens containing stirrups, headed bars and no reinforcement were illustrated. In addition, a discussion regarding the ultimate shear transfer strength was stated, which showed a good agreement between the test results and the design expression suggested previously by Alkatan (2016). Furthermore, GFRP reinforced concrete interfaces were found to maintain considerable post ultimate resistance, especially those with headed bars. The shear transfer strength was discovered to be independent of the shape of the GFRP reinforcement (headed bars or stirrups).

## **CHAPTER 5**

### **CONCLUSIONS AND RECOMMENDATIONS**

#### **5.1 General**

The application of GFRP material as a shear transfer reinforcement was investigated in a prior study (Alkatan, 2016). The present study further explored the feasibility and effectiveness of the GFRP material across the concrete joints with high reinforcement ratios. This research was directed to better understand the behavior of as-cast rough concrete joints intersected by GFRP reinforcement, through an experimental program.

The testing program consisted of two series of push-off specimens. They were large scale specimens with two L-shaped concrete blocks which were cast at different times. The first series of specimens consisted of ten specimens with a shear plane of 250 x 400 mm while the specimens of second series had a shear plane of 250 x 300 mm. Two control specimens have no reinforcement across the shear plane were included in the test program. In addition, two specimens, each contains two steel stirrups crossing its shear plane were also involved in This program. GFRP stirrups and GFRP headed bars were used for the rest of the specimens. The investigated parameters were the reinforcement stiffness ( $E \rho_v$ ) and the shape of the reinforcement (stirrups and headed bars).

## 5.2 Conclusions

The analysis of the test results of the push-off specimens of this study gave more insight into the behavior of concrete joints reinforced with GFRP. The results can be concluded in the following points:

- The shear transfer load-slip behavior of as-cast concrete joints involves three phases, which are; 1) pre-cracking 2) post-cracking and 3) post-ultimate.
- The concrete surface roughness controls the behavior prior to cracking, while the shear reinforcement and the roughness of the cracked interface provide the strength at the post to cracking stage.
- In general, increasing the reinforcement stiffness ( $E\rho_v$ ) lead to an increase in the shear transfer mechanism strength.
- At the ultimate load, a value of 5000 microstrain was found to be a good estimate for the strain of the GFRP bars across the interface.
- Compared to steel reinforced interfaces, those with GFRP reinforcement showed a remarkable shear transfer capacity at higher values of slip.
- The shape of the reinforcement whether it is a headed bar or stirrup did not greatly influence the strength or the behavior prior to ultimate. However, at higher slips, specimens with headed bars showed a notable post peak resistance.
- It was found that the ultimate load for all specimens corresponded to a slip value that did not exceed 1.00 mm.

### 5.3 Future Work

Exploring the performance of the concrete joints using GFRP reinforcement can be further extended. The followings are some ideas for any work in the future:

- The effect of changing the roughness of the interface.
- The influence of the concrete strength on the contribution of the shear plane to the shear transfer strength.
- Using a GFRP reinforcement Inclined to the shear plane.
- The Fatigue performance of concrete joints with GFRP reinforcement.



## REFERENCES

- AASHTO Standard Specifications for Highway Bridges* (17 ed.). (2002). American Association of State Highway and Transportation Officials, ISBN 156051-171-0.
- ACI Committee 711. (1953). Minimum Standard Requirements for Precast Concrete Floor Units (ACI 711-53). *ACI Journal Proceedings*, 50(9), 1-15.
- ACI Committee 711. (1953). Minimum Standard Requirements for Precast Concrete Floor Units (ACI 711-53). *Journal of the American Concrete Institute*, 7-8.
- ACI Committee 318. (1970). *Building requirements for Reinforced Concrete (ACI 318-70) and Commentary (ACI 318R-70)*. Farmington Hills, MI, USA: American Concrete Institute.
- ACI Committee 318. (1999). *Building requirements for Reinforced Concrete (ACI 318-99) and Commentary (ACI 318R-99)*. Farmington Hills, MI, USA: American Concrete Institute.
- ACI Committee 318. (2014). *Building Code Requirements for Structural Concrete (ACI 318-14) and Commentary (ACI 318R-14)*. Farmington Hills, MI, USA: American Concrete Institute.
- Ali, M. A., & White, R. N. (1999). Enhanced Contact Model for Shear Friction of Normal and High-Strength Concrete. *ACI Structural Journal*, 96(3), 348-361.
- Alkatan, J. (2016). *FRP Shear Transfer Reinforcement for Composite Concrete Construction*, M.A.Sc thesis, Department of Civil and Environmental Engineering, University of Windsor, Windsor, Canada.

- Anderson, A. R. (1960, September). Composite Designs in Precast and Cast-in-Place Concrete. *Progressive Architecture*, 41(9), 172-179.
- ASTM C39. (2015). *Standard Test Method for Compressive Strength of Cylindrical Concrete Specimens*. West Conshohocken, PA: ASTM International.
- Beer, F., Johnston, E., DeWolf, J., & Mazurek, D. (2014). *Mechanics of Materials* (7 ed.). McGraw-Hill Education.
- Birkeland, H. W. (1968). Precast and Prestressed Concrete, class notes for course. *University of British Columbia*.
- Birkeland, P. W., & Birkeland, H. W. (1966). Connections in Precast Concrete Construction. *ACI Journal*, 345-367.
- Canadian Standards Association (CSA). (2009). *Carbon Steel bars for Concrete Reinforcement CAN/CSA G30.18-09*. Mississauga, Ontario, Canada: Canadian Standards Association.
- Canadian Standards Association (CSA). (2014). *Canadian Highway Bridge Design Code CAN/CSA-S6-14*. Mississauga, Ontario, Canada: Canadian Standards Association.
- Canadian Standard Association (CSA). (2014). *Design of Concrete Structures for Buildings CAN/CSA-A23.3-14*. Rexdale, Ontario: Canadian Standard Association.
- Harries, K., Zeno, G., & Shahrooz, B. (2012). Toward an Improved Understanding of Shear-Friction Behaviour. *ACI Structural Journal*, 109(6), 835-844.
- Hermansen, B. R., & Cowan, J. (1974). Modified shear-friction theory for bracket design. *ACI Journal Proceedings*, 71(2), 55–60.
- Hofbeck, J., Ibrahim, I., & Mattock, A. (1969). Shear Transfer in Reinforced Concrete. *ACI Journal*, 66(2), 119-128.

- Khan, L., & Mitchell, A. (2002, February). Shear Friction Tests with High-Strength Concrete.
- Li, B., and Maekawa, K. (1987). Contact Density Model for Cracks in Concrete, IABSE Colloquium, Delft, 51-62.
- Loov, R. (1978). Design of Precast Connections. *Paper presented at a seminar orgnized by Compa International Pte, Ltd*, 8 pages.
- Loov, R. E., & Patnaik, A. K. (1994). Horizontal Shear Strength of Composite Concrete Beams with Rough Interfaces. *PCI Journal*, 39(1), 48-69.
- Mansur, M. A., Vinayagam, T., & Tan, K. H. (2008, April). Shear Transfer across a crack in Reinforced High-Strength Concrete. *American Society of Civil Engineers, Journal of Materials in Civil Engineering*, 20(4), 294-302.
- Mast, R. F. (1968, June). Auxiliary Reinforcement in Concrete Connections. *American Society of Civil Engineers, Journal of Structural Division*, 94(ST6), 1485-1505.
- Mattock, A. H. (1974, January). Shear Transfer in Concrete Having Reinforcement at an Angle to the Shear Plane. *American Concrete Institute, Special Publicatio 42*, 17-42.
- Mattock, A. H. (1988, January-February). Reader Comments on "Influence of Concrete Strength and Load History on the Shear Friction Capacity of Concrete Members" by Walraven et al. *PCI Journal*, 33(1), 165-166.
- Mattock, A. H. (1994, Spetember-October). Reader Comments on "Horizontal Shear Strength of Composite Concrete Beams with a Rough Interface" by Loov and Patnaik. *PCI Journal*, 39(5), 106-108.

- Mattock, A. H. (2001, January-February). Shear Friction and High-Strength Concrete. *ACI Structural Journal*, 98(1), 50-59.
- Mattock, A. H., Li, W. K., & Wang, T. C. (1976, January-February). Shear Transfer in lightweight reinforced concrete. *Precast/Prestressed Concrete Institute, PCI Journal*, 21(1), 20-39.
- Mattock, A., & Hawkins, N. (1972). Shear Transfer in Reinforced Concrete-Recent Research. *PCI Journal*, 17(2), 55-75.
- Mau, S., & Hsu, T. (1988, January-February). Reader Comments on "Influence of Concrete Strength and Load History on the Shear Friction Capacity of Concrete Members" by Walraven et al. *PCI Journal*, 33(1), 166-168.
- Patnaik, A. H. (2001, April). Behaviour of Composite Concrete Beams with Smooth Interface. *Journal of Structural Engineering*, 127(4), 359-366.
- Paulay, T., Park, R., & Phillips, M. (1974). Horizontal Construction Joints in Cast-in-Place Reinforced Concrete. *ACI Special Publication SP-4: Shear in Reinforced Concrete, Vol. 2, American Concrete Institute, Detroit*, 559-611.
- Pianca, F., Schell, H., & Cautillo, G. (2005). The performance of epoxy coated reinforcement: experience of the Ontario ministry of transportation. *International Journal of Materials and Product Technology*, 23(3-4), 286-308.
- Raths, C. H. (1977). Reader Comments on "Design Proposals for Reinforced Concrete Corbels" by Mattock, A. H. *PCI Journal*, 22(2), 93-98.
- Saemann, J. C., & Washa, G. W. (1964). Horizontal Shear Connections Between Precast Beams and Cast-in-Place Slabs. *Journal of American Concrete Institute*, 61(11), 1383-1409.

V-ROD. (2016). *Fiber Glass Reinforcement*. Retrieved from  
<http://www.vrod.ca/en/Fiberglass-reinforcement/Civil-Engineering>

Walraven, J., Frénay, J., & Pruijssers, A. (1987, January-February). Influence of Concrete Strength and Load History on the Shear Friction Capacity of Concrete Members. *PCI Journal*, 32(1), 66-84.

Zilch, K. & Reinecke, R. (2001). Capacity of shear joints between high-strength precast elements and normal-strength cast-in-place decks. FIB International Symposium on High Performance Concrete, Orlando, USA.

## **VITA AUCTORIS**

NAME: Mofrhe S. Alruwaili

PLACE OF BIRTH: Syria

YEAR OF BIRTH: 1986

EDUCATION: AL Jouf University, Sakaka, AL Jouf, Saudi Arabia

2007-2012 B.A.Sc. in Civil Engineering

University of Windsor, Windsor, Ontario, Canada

2015-2018 M.A.Sc. in Civil Engineering/ Structural